ANALYSIS AND DESIGN OF HIGH FREQUENCY LINK POWER CONVERSION SYSTEMS FOR FUEL CELL POWER CONDITIONING

A Dissertation

by

YU JIN SONG

Submitted to the Office of Graduate Studies of
Texas A&M University
in partial fulfillment of the requirements for the degree of

DOCTOR OF PHILOSOPHY

August 2004

Major Subject: Electrical Engineering

ANALYSIS AND DESIGN OF HIGH FREQUENCY LINK POWER

CONVERSION SYSTEMS FOR FUEL CELL POWER CONDITIONING

A Dissertation

by

YU JIN SONG

Submitted to the Office of Graduate Studies of
Texas A&M University
in partial fulfillment of the requirements for the degree of

DOCTOR OF PHILOSOPHY

Approved as to style and content by:

Prasad N.Enjeti (Chair of Committee)	
Chanan Singh (Member)	Daren B.H. Cline (Member)
Aniruddha Datta (Member)	Chanan Singh (Head of Department)

August 2004

Major Subject: Electrical Engineering

ABSTRACT

Analysis and Design of High Frequency Link Power Conversion Systems

for Fuel Cell Power Conditioning. (August 2004)

Yu Jin Song, B.S., Yonsei University, Seoul, Korea;

M.S., Yonsei University, Seoul, Korea

Chair of Advisory Committee: Dr. Prasad N. Enjeti

In this dissertation, new high frequency link power conversion systems for the fuel cell power conditioning are proposed to improve the performance and optimize the cost, size, and weight of the power conversion systems.

The first study proposes a new soft switching technique for the phase-shift controlled bi-directional dc-dc converter. The described dc-dc converter employs a low profile high frequency transformer and two active full-bridge converters for bi-directional power flow capability. The proposed new soft switching technique guarantees soft switching over wide range from no load to full load without any additional circuit components. The load range for proposed soft switching technique is analyzed by mathematical approach with equivalent circuits and verified by experiments.

The second study describes a boost converter cascaded high frequency link direct dc-ac converter suitable for fuel cell power sources. A new multi-loop control for a boost converter to reduce the low frequency input current harmonics drawn from the fuel cell is proposed, and a new PWM technique for the cycloconverter at the secondary to

reject the low order harmonics in the output voltages is presented. The performance of the proposed scheme is verified by the various simulations and experiments, and their trade-offs are described in detail using mathematical evaluation approach.

The third study proposes a current-fed high frequency link direct dc-ac converter suitable for residential fuel cell power systems. The high frequency full-bridge inverter at the primary generates sinusoidally PWM modulated current pulses with zero current switching (ZCS), and the cycloconverter at the secondary which consists of only two bidirectional switches and output filter capacitors produces sinusoidally modulated 60Hz split single phase output voltage waveforms with near zero current switching. The active harmonic filter connected to the input terminal compensates the low order input current harmonics drawn from the fuel cell without long-term energy storage devices such as batteries and super capacitors.

To my Parents

To my wife, and Chae Eon and Annie

ACKNOWLEDGMENTS

I have been very fortunate to have had the guidance and support of Dr. Prasad Enjeti throughout my research. On numerous occasions, it was his experience, suggestions and encouragement that made progress possible. For this, I would like to express my gratitude to him. I would like to thank my committee members, Dr. Singh, Dr. Datta and Dr. Cline for their time and concern.

I would like to thank to my parents for their love, support and encouragement. Finally, I wish to express my deepest gratitude to my wife, Hee Young. Her love, support, and patience during my long hours of research made these years worthwhile.

TABLE OF CONTENTS

CHAPTER Page

LIST OF FIGURES

FIGURE Page

LIST OF TABLES

CHAPTER I

INTRODUCTION

1.1 Introduction

In the fast decade, there is a remarkable progress in high frequency switching power electronics, which are mainly concerned with system technology using new power semiconductor devices and signal processing/control devices. It has been made on the basis of the application-oriented research and development of high frequency switch mode power conversion circuits and systems with high frequency link employing power semiconductor device modules for high frequency switching control such as MOSFETs, IGBTs, Bi-MOS cascade and/or cascade transistors/thyristors, GTO thyristor and promising MOS controlled thyristors (MCTs) including intelligent power ICs [1].

Static power conversion systems commonly utilize a dc link for distribution of power and temporary energy storage (for decoupling) in the system. A factor behind the wide spread use of dc as a link has been the ease and effectiveness with which the energy storage function can be implemented in a dc link. Electrolytic capacitors provide low cost, high density energy storage in popular dc voltage link systems. DC inductors perform a similar function, although somewhat less effectively, in dc current link systems frequently employed in high power ac drives. In addition, relatively simple converter topologies have been available for power conversion to and from dc [2].

This dissertation follows the style of *IEEE Transactions on Industry Applications*.

With continued progress in the development of power components and devices, improvements in the performance capabilities of dc link systems are to be expected. However, dramatic gains in such attributes as faster system response, higher converter bandwidths, increased output frequencies, improved power densities, reduction in audible and electrical noise associated with the power conversion process, increased safety, and others will require advances in power conversion system configurations in addition to continued progress to power conversion subjects the system to some basic constraints which ultimately limit its overall performance.

A major limitation of the dc link approach is that voltage amplitude changes and electrical isolation, to some extent protection are inherently difficult to achieve. As a result, a large number of dc link systems either avoid voltage shifting and isolation functions entirely or implement these outside of the dc link at a penalty of size, weight and efficiency.

The hard switching contributes in making the dc link power converters simple, but it is largely responsible for high levels of losses and device stresses during switching intervals. As a result, switching frequencies in traditional dc converters have failed to rise, in turn, limiting output frequencies, converter bandwidths, power densities and other such capabilities related to switching frequency. Also high device stresses have had an adverse effect on the reliability of these power converters. An indirect consequence of this limitation has been that device manufactures have spent a considerable amount of development effort to make devices capable of withstanding

high switching stresses resulting in undesirable compromises in other areas of device performance.

As advanced power electronic components and high speed controllers are available, high frequency link power conversion systems employing a high frequency transformer as a link are gaining increasing attention as an alternative to the conventional dc link power conversion systems. The alternative approach of utilizing a high frequency link has several advantages. A power conversion system with a high frequency link can use transformers within the link to meet possibly conflicting voltage level requirements in the system. With adjustable link voltage, each converter in the system can be operated from a link voltage that is optimal for its needs. A high frequency link provides increased flexibility in power distribution since entire sections of the link can be operated at the voltage levels higher or lower than that of the rest of the system. Electrical isolation is readily achieved to allow safer grounding practices and more effective noise suppression in the system. An alternating link voltage also makes it easier to detect and quickly isolate faulty converters in the system and thus, further increases the safety and reliability of the entire system. The penalty of size, weight and efficiency that would normally be associated with the use of low frequency transformers in the power conversion system is minimized by choosing a high value (20 kHz or above) for the link frequency.

In general, the semiconductor power conversion circuits and system with a unidirectional or a bidirectional power flow regulation schemes using high frequency link concepts not only possess a high power density adaptability in practical

requirement, but also include high efficient and first response power conversion characteristics and lowered acoustic noise and reduced EMI noise as compared with the conventional high frequency carrier based sine wave PWM power conversion systems with current feedback or current adaptive scheme using low frequency transformer link, which are extremely bulky in size and weight and become non cost-effective.

As next generation ac power supply and distributed power systems in high-tech modern power electronics technology fields, the high performance and high power density dc-ac power conversion systems with a high frequency link using new power semiconductor and circuit component devices have become of major interest recently in telecommunication and a decentralized residential power generation systems with an renewable new energy sources and an energy storage battery link. Especially, so called new energy systems including photo voltaic system, fuel cell generation systems and wind turbine generation systems and so on combined energy storage system using flywheels or batteries are expected to be widely spread to form a distributed power system. Wind turbines and photovoltaic cells are well known and matured technologies but both have an obvious disadvantage: these systems deliver power only when the wind blows/the sun is shining. Thus, these technologies cannot be used as primary power supply in the grid. However, unlike wind turbines and photovoltaic cells, fuel cells can provide the power (electrical and thermal) continuously as long as the fuel and air are supplied, and are one of the systems closest to practical application for distributed power systems.

1.2 Overview of fuel cells

Relative environmental reasons for the use of fossil fuels have been creating, along the years, a steadily increasing demand for new conversion technology and system of non-pollutants energy generation. Within this context, fuel cells have been showing up as a highly promising alternative for their high efficiency, low aggression to the environment, modularity and superior reliability and durability in automotive, stationary and space applications. [3]

Fuel cells are electrochemical devices that convert a fuel's chemical energy directly to electrical energy with high efficiency. A fuel cell consists of two electrodes and an electrolyte (Fig. 1.1). On a side of the cell, referred as the anode, the fuel is supplied under certain pressure.

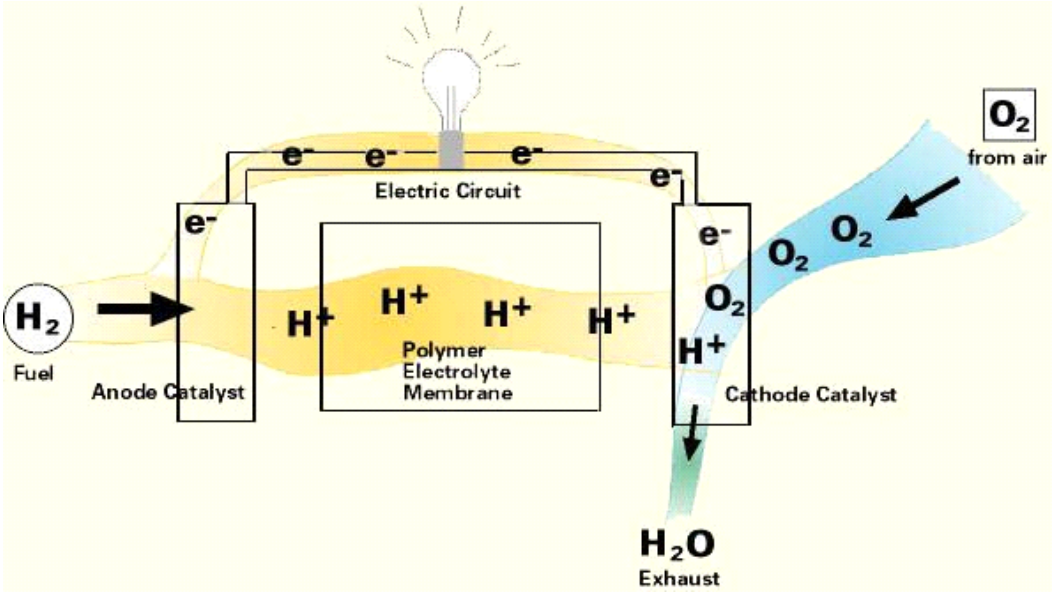

Fig. 1.1 Basic PEM fuel cell mechanism [4].

The pure gas H_2 or the other types of fuel with reformer is used as a fuel. The fuel spreads through the electrode until it reaches the catalytic layer of the anode where it reacts to form protons and electrons as shown below in the reaction:

$$H_{2(g)} \rightarrow 2H^+ + 2e^- \tag{1.1}$$

The protons are transferred through the electrolyte (solid membrane) to the catalytic layer of the cathode. On the other side of the cell, the oxidizer (O_2 or air) flows in the channels of the plate and it spreads through the electrode until it reaches the catalytic layer of the cathode. The oxygen is consumed with the protons and electrons and the products, liquid water, is produced with residual heat in the surface of the catalytic particles. The electrons, which can not pass through the membrane, flow from the anode to the cathode via the external electric circuit, delivering power to the electric circuit in the process. The electromechanical reaction that happens in the cathode is:

$$2H^+ + 2e^- + \frac{1}{2}O_2 \rightarrow H_2O + heat \tag{1.2}$$

Then, the full chemical fuel cell reaction of is:

$$H_2 + \frac{1}{2}O_2 \rightarrow H_2O + heat + electricity \tag{1.3}$$

There are many types of fuel cells, differing in components and materials, and their applications vary from the portable and the transportation to the stationery and the space. An overview of the major designs is illustrated in Table 1.1.

Table 1.1 Types of fuel cells [4].

	Fuel cell type			
	Polymer electrolyte membrane	Phosphoric acid	Molten carbonate	Solid oxide
Electrolyte	Ion exchange membrane	Phosphoric acid	Alkali carbonates	Yttria stabilized zirconia
Operating temperature(˚C)	80	200	650	800-1000
Charge carrier	H^+	H^+	CO_3^{2-}	O^{2-}
Electrolyte state	Solid	Immobilized liquid	Immobilized liquid	Solid
Cell hardware	Carbon- or metal-based	Graphite -based	Stainless steel	Ceramic
Catalyst	Platinum	Platinum	Nickel	Perovsites
Cogeneration heat	None	Low quality	High	High
Efficiency (%)	<40	40-45	50-60	50-60

The V-I characteristic of a single cell is shown in Fig. 1.2. The theoretical EMF of a cell at zero current and 80°C and 1 atm gas pressure is V_o=1.16V. As the current density increases, the actual voltage at the electrical terminals drops.

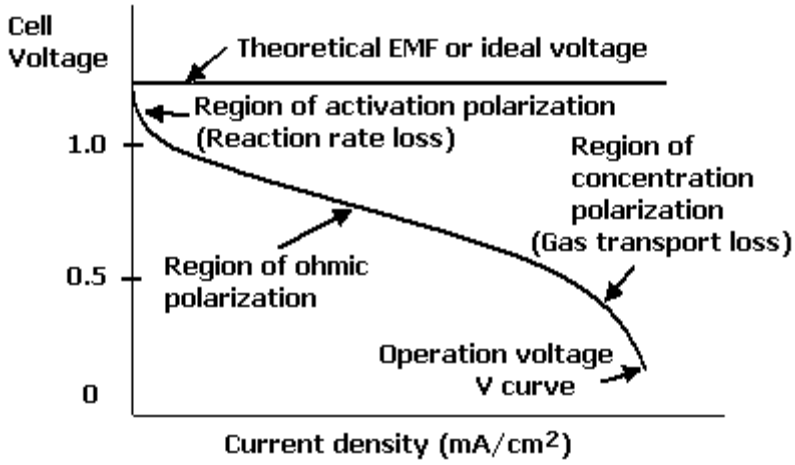

Fig. 1.2 V-I characteristic of a cell [3].

The fuel cell efficiency is given by

$$\eta = \frac{V \bullet I}{V_o \bullet I} = \frac{V}{V_o}, \tag{1.4}$$

and is simply equal to the ratio of the terminal voltage to the theoretical EMF for the cell. The energy lost is transformed into heat. In the V-I characteristic three separate regions can be identified:

- Region of activation polarization. For very small currents the voltage drops rapidly as current increases.
- Region of ohmic polarization. In this region, the voltage decreases linearly with current. Clearly, a Thevenin equivalent circuit with a resistance equal to the slope of the curve is appropriate in this region. This is the normal operating region of a fuel cell.

- Region of transportation polarization. When current exceeds a certain value, the voltage collapses rapidly. This knee of the V-I characteristic represents the upper limit of the safe operation for the cell. Given significant losses, prolonged operation in this region may damage the fuel cell

The voltage from one single cell is approximately 0.7V. As in batteries, cells are stacked in series to provide higher voltages. A large number of series cells leads to reduced reliability, since, if a single cell fails open, the entire stack stops functioning because the current flow is interrupted.

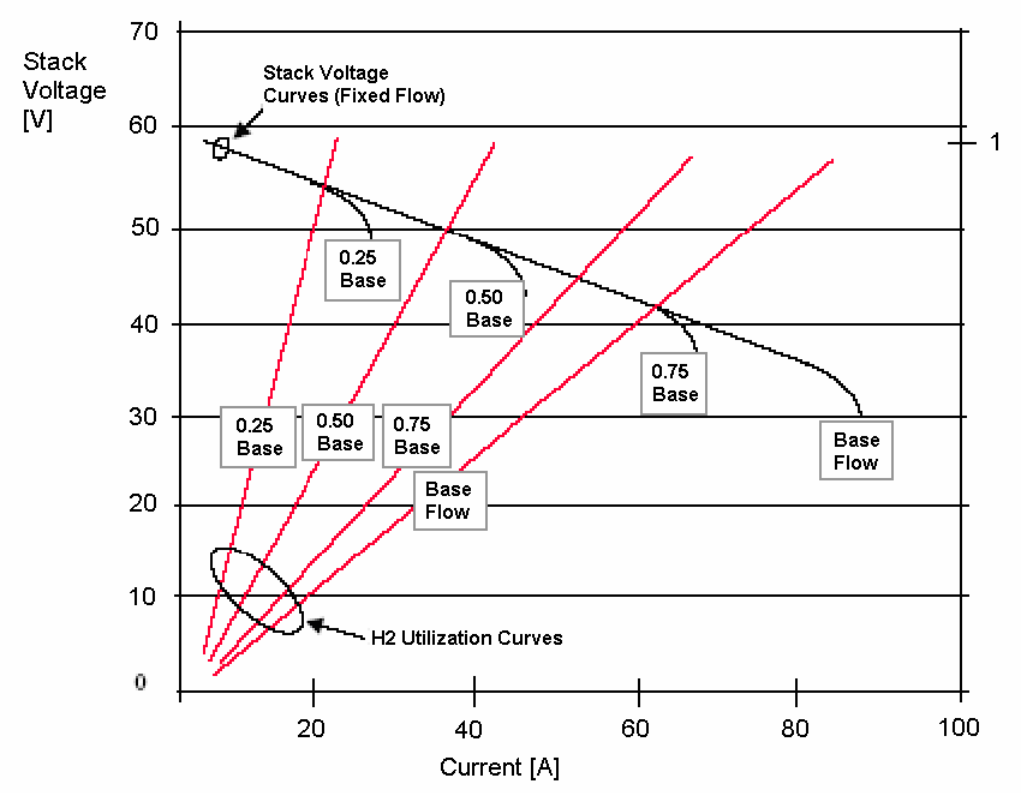

Fig. 1.3 Static characteristics of the fuel cell stack for various level of hydrogen flow [3].

The static characteristic of the fuel cell stack for different values of hydrogen flow is shown in Fig. 1.3. The fuel cell voltage reaches the knee point and collapses when the hydrogen utilization approaches 100%, and the knee point moves to higher current levels when the hydrogen flow is higher. The dc voltage generated by fuel cell stacks varies widely depending on the load change, and the fuel cell response time to changes in power demand is slow and varies from few seconds to few minutes. The mismatch between fuel cell time constant and typical electrical time constants of a domestic power system clearly points to the need of buffer energy storage in the interface system. Since the hydrogen of fuel cell system has to be adjusted to peak current demand, a low frequency current ripple is undesirable. In addition, a current back feed into the fuel cell must be avoided because the fuel cell can be damaged by a reverse current flow.

A fuel cell system consists of a fuel cell stack plus a number of auxiliary systems needed for its operation, such as an air compressor to provide pressurized air flow through the cathode, a water-cooling system to remove heat from the stack, valves to control the hydrogen flow through the anode, and so on. Fuel cell operation is a delicate balance of gas flows and chemical reaction rates. Sudden electrical load changes can cause problems. For example, a sudden increase in electrical load may cause the membrane to flood. The water produced at the cathode is not removed fast enough and not enough oxygen is able to reach the cathode catalyst sites though the excess liquid water. Therefore, the fuel cell operation point should be adjusted as a function of electrical load for efficient fuel cell operation. By doing this it is possible to: reduce the

power losses in the air compressor at light loads, reduce losses of hydrogen in an open fuel cell system, and adjust the reformer rate of operation depending on hydrogen utilization. Since these adjustments involve mechanical systems, the response time of the fuel cell to varying electrical load is slow. This slow dynamic response is one of most significant challenges in designing fuel cell power conversion system [3].

1.3 Fuel cell power systems

A fuel cell power system designed for power conditioning should have following characteristics: (1) allowable for wide output voltage regulation of fuel cell; (2) fast transient response; (3) high power density; (4) high efficiency; (5) available for isolated operation [5].

A fuel cell power system consists of three main sections:

- fuel processor where the fuel is converted to hydrogen-rich gas
- fuel cell power section, consisting of a stack of fuel cells where the hydrogen gas and oxidants are combined to produce direct current electricity and heat
- power conditioning unit (inverter/converter) to convert the fuel cell power to ac or dc depending on the nature of the load.

, and a typical fuel cell power system consists of several components (Fig. 1.4).

- a fuel processor: gasoline or methanol reformer (if direct hydrogen is used, than a hydrogen storage tank is required)

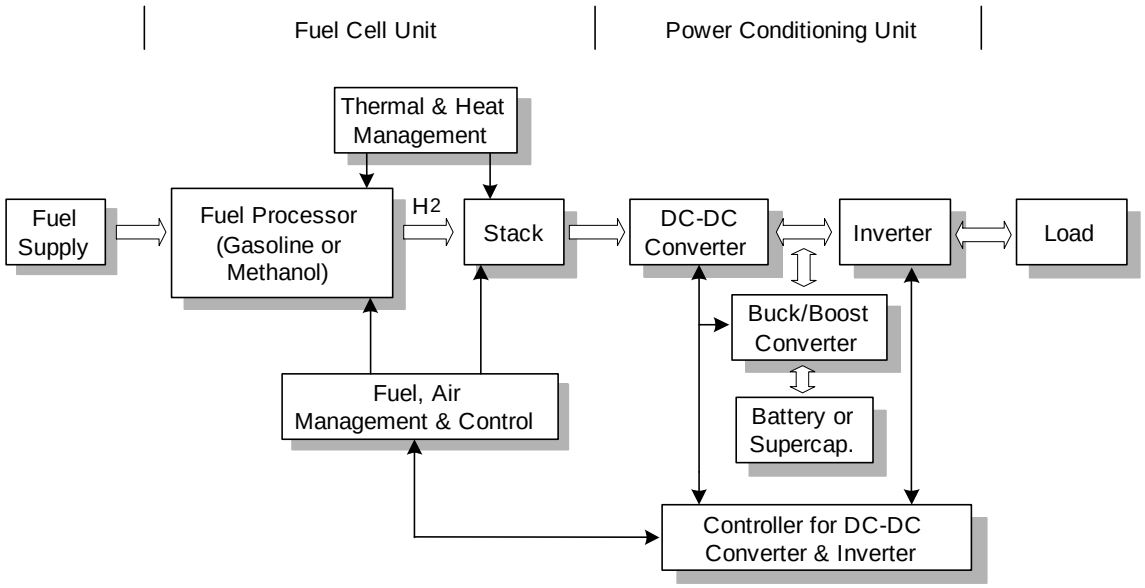

Fig. 1.4 Fuel cell power system.

- the fuel cell stack, which produces the electricity, and an air compressor to provide pressurized oxygen to the fuel cell
- a cooling system to maintain the proper operating temperature
- a water management system to manage the humidity and moisture in the system (to keep the fuel cell membrane saturated and at the same time prevent water being accumulated at the cathode)
- a dc-dc converter to condition the output voltage of the fuel cell stack
- an inverter to convert the dc to low frequency ac voltage
- a battery or a supercapacitor is generally connected to the fuel cell power system in parallel to provide supplemental power for starting the system.

As fuel cell produces dc output voltage that is unregulated, a dc-dc converter that placed between the fuel cell module and the inverter boosts and regulates the output

voltage of the fuel cell and supplies the constant dc voltage to the inverter, which allows the inverter to operate optimally, and the inverter produces PWM modulated ac output voltages for the load. The bidirectional power flow buck/boost converter charges the battery or supercapacitor during reverse power flow by regenerative breaking and provides the supplemental power during start-up and load change.

1.4 Review of previous work

From the view point of power conversion, the power converters mentioned above play significant rolls in the fuel cell power system for distributed power system applications. The required properties for the power converters for distributed power systems are as follows:

- High efficiency in power conversion
- High power density
- Small size and light weight
- Electrical isolation to avoid electric leak and /or electric shock
- Bi-directional power flow
- Low EMI

The high frequency link power conversion technique is attractive for fuel cell power system applications where the properties mentioned above are prerequisite. The high frequency link power conversion systems employing a high frequency transformer is suitable for single phase dc-ac or three phase dc-ac conversion applications, and is profitably applicable to the small-scale or medium-scale high quality power generation

system powered from renewable energy source such as fuel cell where the galvanic isolation and high conversion efficiency are required.

1.4.1 High frequency power conversion systems

Fig. 1.5. schematically illustrates several typical topologies of high frequency link dc-ac power conversion systems employing a high frequency transformer. There are two types of high frequency link dc-ac converters; a dc-dc converter type dc-ac converter and a cycloconverter type dc-ac converter. Both can be a current-fed converter or a voltage-fed converter. A current-fed dc-ac converter requires less input filtering in order to minimize the high frequency current ripple drawn by the dc-ac converter because the inductor is placed at the input terminal. The dc-dc converter of dc-dc converter type consists of a high frequency inverter, a high frequency transformer, a diode rectifier and a low pass filter and an inverter, where the high frequency transformer step-up the voltage/current pulse input and also provides a galvanic isolation between the input and the output (Fig. 1.5 (a)).

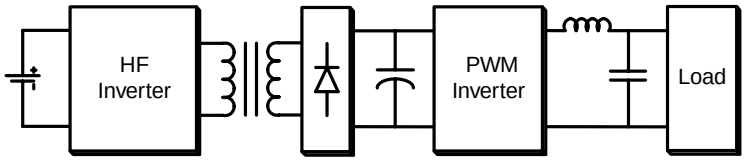

(a)

Fig. 1.5 High frequency link dc-ac converters. (a) DC-DC converter type. (b) PWM inverter type. (c) PWM cycloconverter type. (d) Dual high frequency link type.

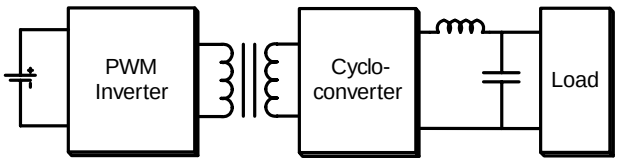

(b)

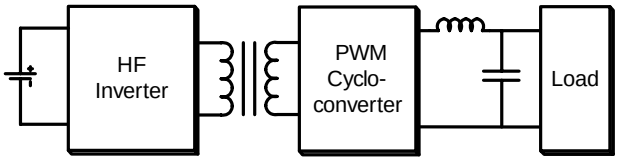

(c)

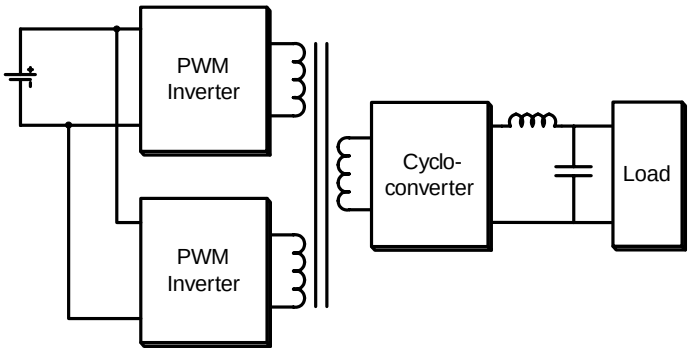

(d)

Fig. 1.5 Continued.

The dc input voltage is converted to a regulated higher dc voltage by the dc-dc converter, and an inverter produces PWM modulated low frequency ac output voltages. The output voltage of sinusoidal PWM inverter at the final stage is controlled through the instantaneous voltage feedback loop independently of dc-dc converter operation. The dc-dc converter type has been adopted widely in designing distributed power system because of its ease and effectiveness with which the energy storage function can be

implemented in a link. Electrolytic capacitors provide low cost, high density energy storage in popular dc-dc converter type high frequency link systems. However, this kind of configuration is applicable to only the systems of which active power flow is unidirectional, and the energy storage element makes it bulky and its several power conversion steps degrade the power conversion efficiency [6-10].

The cycloconverter type is roughly classified into three; a PWM inverter type, a PWM cycloconverter type and a dual high frequency link type. The cycloconverter type dc-ac converter consists of an inverter at the primary side, a cycloconverter at the secondary side and a high frequency transformer between the two converters. Using this configuration, a compact-size direct dc-ac converter can be constructed by eliminating the dc link capacitor, and it can be operated with high conversion efficiency due to the reduced power conversion step, but it is not easy to process the energy stored into the leakage inductance of high frequency transformer and stray inductance of wire. Fig. 1.5 (b) shows a PWM inverter type high frequency link dc-ac converter. In this system, the input dc voltage is converted into high frequency voltage having low frequency ac output component by a PWM inverter isolated by a high frequency transformer and converted into low frequency ac voltage by a cycloconverter. This system lacks flexibility since the PWM control is executed by the high frequency PWM inverter at the primary. When constructing a three-phase output system, three sets of PWM inverter and cycloconverter are necessary. Fig. 1.5 (c) presents a PWM cycloconverter type high frequency link dc-ac converter system. In this configuration, the dc input voltage is converted into high frequency 50% duty ratio rectangular voltage

by an inverter isolated by a high frequency transformer and converted into low frequency ac voltage by a PWM cycloconverter. This system has a good flexibility especially for a multi-phase output systems because the output of the inverter is not controlled and the multi-phase PWM output can be obtained by a multi-phase cycloconverter. Ranganathan, Ziogas and Stefanovic have suggested an alternative approach to power conversion employing dual high frequency voltage links [11] (Fig. 1.5 (d)). The proposed configuration combines two independent high frequency voltage outputs to produce an intermediate high frequency voltage that is amplitude modulated with the desired low frequency voltage which is then recovered by using synchronous rectification/inversion. This scheme allows independent regulation of both the voltage and the frequency of the synthesized low frequency voltage signal.

The various types of cycloconverter type three phase dc-ac converter were presented for UPS applications in 1990s [12-13], and provided a possible solution to build a compact high frequency dc-ac converter which has high conversion efficiency by employing high frequency transformer and cycloconverter. Several single-phase schemes adopting high frequency link have been proposed recently in order to provide a low cost power conversion system for distributed power system application with renewable energy sources [7-10], but those scheme did not present an active solution for eliminating low frequency input harmonics drawn by high frequency link dc-ac converters and low frequency harmonics of the ac output voltage caused by dc voltage ripple.

1.4.2 Feasibility of high frequency link power conversion system for fuel cell applications

A typical output voltage of fuel cells is 36V to 60V depending on the load condition. A power conversion system for fuel cell applications requires a capability of boosting the low output voltage of fuel cell in order to obtain the 120V/240V split single phase or 208V three phase at the output, and a electrical isolations is a prerequisite for safety reason in distributed power system. These requirements can be achieved easily by a high frequency power conversion technique. The high frequency link power conversion technique provides a solution to construct a compact high frequency link dc-ac converter where the high frequency transformer step-up the fuel cell output voltage and provides a galvanic isolation.

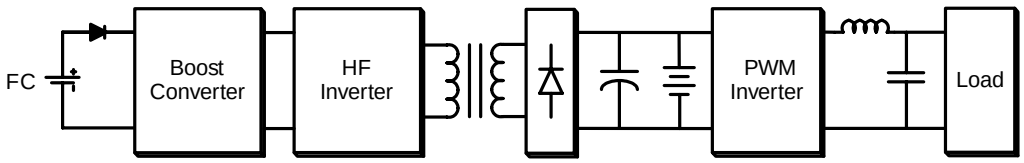

(a)

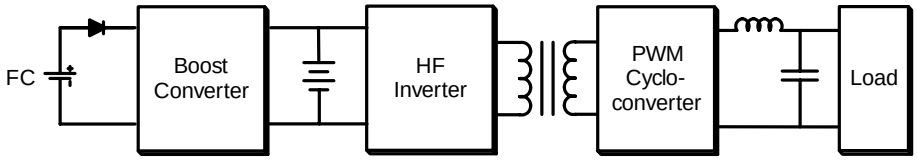

(b)

Fig. 1.6 High frequency link dc-ac converters for fuel cell applications. (a) DC-DC converter type. (b) Cycloconverter type.

There are two possible candidates for fuel cell power systems; a DC-DC converter type and a cycloconverter type (Fig. 1.6). Fig. 1.6 (a) shows the dc-dc converter type high frequency link dc-ac converter. Since the dc voltage generated by a fuel cell varies significantly depending on the load change, it is required to boost and regulate the fuel cell voltage. The high frequency link transformer needs to be designed to accommodate the lowest fuel cell voltage level. During the normal operation the nominal input voltages are typically much higher than the minimum value and the transformer does not operate optimally. Therefore, the boost converter set-up the fuel cell voltage and supplies a constant dc voltage to the input terminal of high frequency inverter at the primary, which allows the inverter to operate with a fixed duty ratio and does transformer to operate efficiently**.** The isolated dc-dc converter can be a current-fed type or a voltage-fed type and its topology can be in push-pull connection or full bridge connection. A dual half-bridge inverter or a full-bridge inverter can be adopted as an inverter at the output stage. The power conversion step includes dc to ac, ac to dc and dc to ac. Several power conversion steps and dc link capacitors of the dc-dc converter type result in low conversion efficiency low and bulky size. As explained in the first section, the slow dynamics of fuel cell requires buffering in the interface system. Since the power flow of the dc-dc converter type is unidirectional, a battery or a suppercapacitor can be connected in parallel at the secondary. Except for the potential high cost, the suppercapacitor has merit, because the fuel cell voltage droops significantly under load, allowing significant energy to be extracted from it. The high voltage batteries of dc-dc converter type connected in parallel with a dc link capacitor naturally provides buffering

between the fuel cell and the output. From the control point of view, the output inverter stage can have fast dynamics to correct against load transients, whereas the isolated dc-dc converter stage can be operated so that the current taken from the fuel cell does not exceed the maximum available fuel cell current. The status of charge of the battery determines the power request from the inverter system to the fuel cell, so that the fuel cell output slowly adjust to load variations. However, the use of high voltage (200V) battery connected in serial may present serous charge equalization problem. Some type of active battery balancing scheme is necessary for system reliability.

Fig. 1.6 (b) presents a cycloconverter type high frequency link dc-ac converter for fuel cell applications. A boost converter acts as a buffer between the fuel cell and the battery. A high frequency inverter in push-pull connection or full-bridge connection generates high frequency ac voltage, which is stepped up by the high frequency link transformer. A cycloconverter consisting of bidirectional switches, SCR or IGBT, produces 60Hz output voltage. The power conversion step is reduced and a bulky dc link capacitor is removed, which allows construct a low profile direct dc-ac converter with high efficiency. Since the power flow of the cycloconverter type is bidirectional, the battery is placed between the boost converter and the inverter at the primary. The battery provides power to the following converter immediately after the stored energy in the output capacitor of boost converter is consumed during load transient. The boost converter precisely controls the current taken from the fuel cell ensuring that the maximum allowable current is not exceeded.

Another solution to compensate the slow dynamics of the fuel cell is to connect an active converter with battery to the fuel cell in parallel (Fig. 1.7).

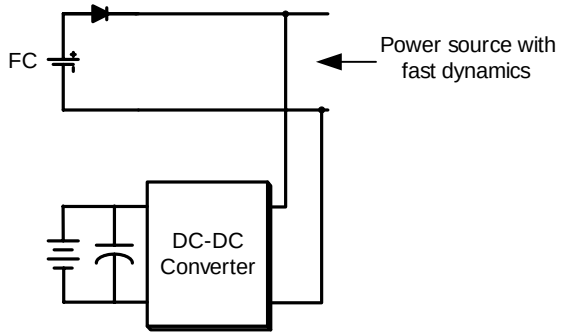

Fig. 1.7 DC-DC converter with battery for slow dynamics compensation.

The active converter should have a capability of bidirectional power flow, and its functions are as follows; when the output requires more power than the fuel cell can provide, the active converter supplies the excess power taking it from the battery; otherwise the active converter keeps the battery charged. In addition, the active converter with a capacitor connected to battery in parallel can be used as an active harmonic filter to eliminate the low frequency current ripple drawn from the fuel cell by the high frequency link dc-ac converter [3].

1.5 Research objectives

As mentioned in the earlier section, the high frequency link power conversion system is one of most promising candidates for the fuel cell power system to satisfy the required properties for the distributed power system applications.

The main objective of this research is to investigate and study the high frequency link power conversion systems, and design and develop new high frequency link power conversion systems for the fuel cell power system to improve the performance and optimize the cost, size, and weight of the power conversion systems. The proposed high frequency link power conversion systems employ a high frequency link transformer replacing a bulky low frequency transformer and realize a compact high frequency power conversion system which has the characteristics such as galvanic isolation, high power density, high conversion efficiency and bidirectional power flow. The proposed systems employ state of the art power electronics devices and design new topologies and switching strategies to achieve the improved performance and efficiency and optimize the cost and volume.

In the first study, high frequency power conversion systems are explored and investigated for their suitability in the fuel cell power conversion systems.

In the second study, a new soft switching technique for the bi-directional power flow, full-bridge dc-dc converter is proposed in order to reduce the switching loss and EMI, which is applicable to the buck/boost converter to charge the battery or supercapacitor during reverse power flow by regenerative break and supply supplemental power during start-up and load change. The proposed soft switching technique realizes soft switching over wide range from no load to full load without any additional circuit component, which is analyzed mathematically using the equivalent circuits of each operation modes, and its performance is proved by the experiment results.

In the third study, a boost converter cascaded high frequency link direct dc-ac converter for fuel cell application is proposed. A front-end boost converter is employed to boost and regulate the fuel cell output voltage varies from 36V to 60V depending on the load, and supply the regulated constant voltage to the high frequency link dc-ac converter at the second stage, which allow it to operate optimally. A new multi-loop control strategy for the boost converter is designed to reduce the low frequency current ripple drawn from the fuel cell by the dc-ac converter and improve the performance of fuel cell power system. A cycloconverter with high frequency transformer at the secondary is designed to reduce the size and weight by eliminating a bulky intermediate dc link capacitor and improve the power conversion efficiency by reducing the power conversion step. The new PWM switching technique for the cycloconverter is developed to reduce the low order harmonics of output voltage and current caused by the low frequency voltage ripple of the dc bus and the conventional PWM technique assuming the ripple free dc voltage, which guarantees a high quality output and reduces the LC output filter requirement.

Finally, a current-fed high frequency link direct dc-ac converter with active harmonic filter is proposed with presenting a possible way to build a compact dc-ac converter with high efficiency. The proposed current-fed high frequency link direct dc-ac converter generates the split single phase ac outputs with zero current switching from the fuel cell powered dc source in a single power conversion stage. The proposed converter configures a cost-effective topology employing a simple cycloconverter consisting of two bidirectional switches and two capacitor output filters only at the

secondary. The active harmonic filter makes the compensation current and eliminates the low frequency input harmonic current drawn from the fuel cell without long-term energy storage devices such as battery or supercapacitor. The operation modes of each topology and their control schemes are detailed.

1.6 Dissertation outline

The content of this dissertation is organized in the following manner:

In Chapter I, the general information about the high frequency link power conversion systems is introduced at first, and the overview of fuel cell and the fuel cell power systems are described. The previous works of high frequency power conversion systems are reviewed. Their advantages and disadvantages are detailed, and their suitability in the fuel cell power conversion systems is investigated. Finally, research objectives are presented and discussed.

In Chapter II, a new soft switching technique for the bi-directional power flow, full-bridge dc-dc converter is proposed in order to reduce the switching loss and EMI.

The load range for proposed soft switching technique is analyzed mathematically using the equivalent circuits of each operation modes, and its performance is discussed with the experiment results.

In Chapter III, a boost converter cascaded high frequency link direct dc-ac converter for fuel cell power systems is presented. The new multi-loop control scheme for the boost converter and the new PWM switching technique for the cycloconverter are

described with mathematical analysis, and their performance is discussed with the various simulation results and experiment results.

Chapter IV presents a current-fed high frequency link direct dc-ac converter with active harmonic filter for the fuel cell power generation system applications. The operation modes of dc-ac converter and active harmonic filter and their control strategies are detailed, and the various simulation results are provided to validate the proposed scheme.

Chapter V summarizes the contributions of this research work in the area of high frequency link power conversion systems for fuel cell power system applications. Finally, some suggestions are included for further work.

CHAPTER II

A NEW SOFT SWITCHING TECHNIQUE FOR BIDIRECTIONAL POWER FLOW, FULL-BRIDGE DC-DC CONVERTER

2.1 Introduction

The dual active full-bridge dc-dc converter shown in Fig. 2.1 (a) is a viable candidate for high frequency power conversion system in space power and electric vehicle. This type of power conversion has been shown to possess attractive features such as high power density, high efficiency, small filter components and bi-directional power flow [14]. Another important feature of this bidirectional scheme is zero voltage switching (ZVS), which allows reduction of the switching losses dramatically. ZVS relies on the primary current of the transformer, I_p, to discharge and charge the parasitic capacitances of the switch ($C_{1\text{-}4}$) before turning on/off. As shown in Fig. 2.1.(b), during the switching transition at right leg the, the primary current of the transformer is sufficient to discharge the parasitic capacitance of the switch for ZVS, while during the switching transition at left leg, the primary current reduces and changes its direction under light load. Therefore, the energy available from the leakage inductance of the transformer, L_{lk}, to discharge and charge the parasitic capacitances of the switches during the switching transition at left leg is less, and results in a failure to achieve ZVS under light load condition because the energy available for ZVS depends on the load current [15].

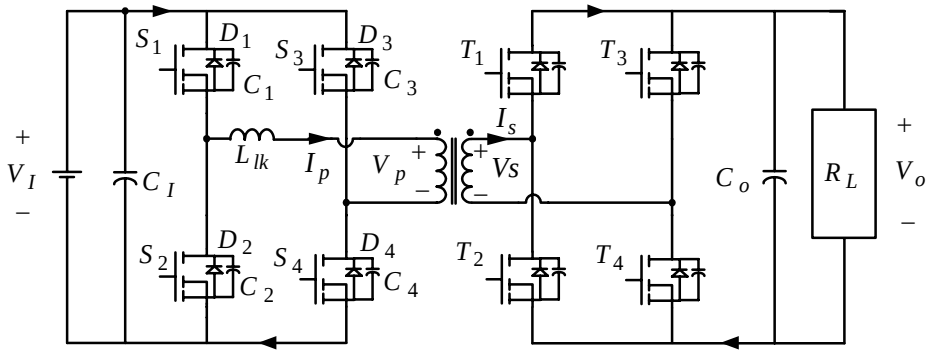

(a)

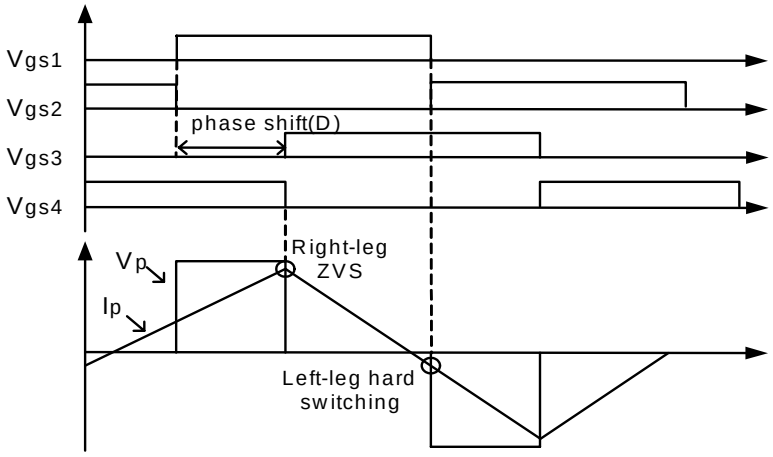

(b)

Fig. 2.1 Dual active full-bridge dc-dc converter and its switching waveform. (a) Topology. (b) Switching waveforms of the converter.

Many methods have been proposed to extend the load range for ZVS, and there are two main approaches. The first is to use additional circuit components such as an extra inductor, a saturable inductor in series with the primary transformer and a snubber circuit [16-18]. This approach, while extending the load range for ZVS, results in

significant conduction losses or increases the design cost. The other approach is to employ zero current switching (ZCS) at the left leg transition and ZVS at the right leg transition without additional hardware component. This approach also extends the load range for soft switching, but there is a region between minimum load for ZVS and maximum load for ZCS at left leg, where the switches of the left leg neither work under ZCS nor ZVS [19]. This paper proposes a new soft switching technique using switching signals with a variable duty ratio depending on the phase shift amount.

The advantages of the proposed soft switching technique are as follows

- It doesn't require any additional circuit components.
- It realizes the soft switching over a wide range from no load to full load.
- No freewheeling interval reduces the circulating current, hence resulting in the reduction of conduction losses.

2.2 Principle of circuit operation and soft switching

As the switching signal waveforms, $V_{gs1\text{-}4}$, of the switch $S_{1\text{-}4}$ shown in Fig. 2.2, the switches of converter with a conventional switching scheme are operated at fixed 50% duty ratio. The primary current of the transformer, I_P, is sufficient to discharge and charge the capacitances (C_3, C_4) during the switch transition at right leg and turns on S_3 under zero voltage. However, during the switching transition at the left leg, the primary current of the transformer changes its polarity and decreases, and is not sufficient to discharge/charge the capacitances (C_1, C_2) under light load, which results in hard switching of S_2 at left leg.

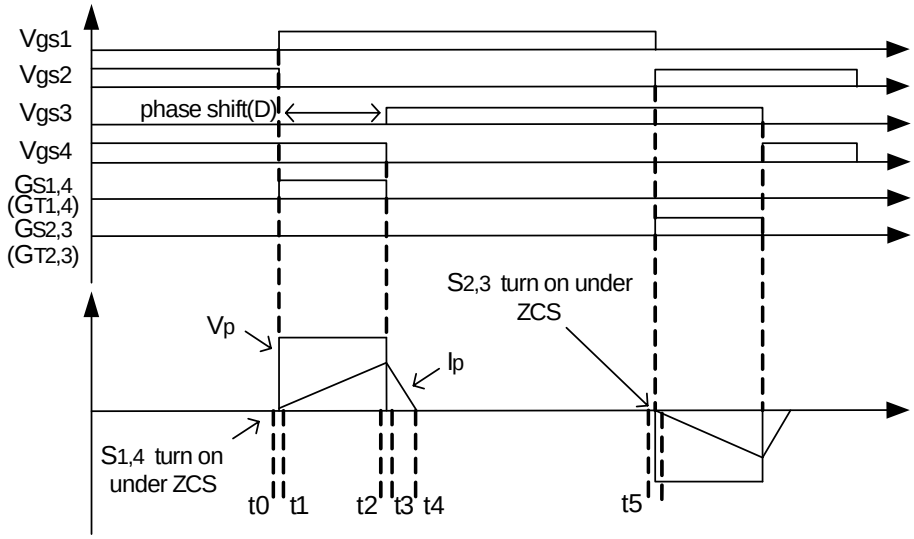

(a)

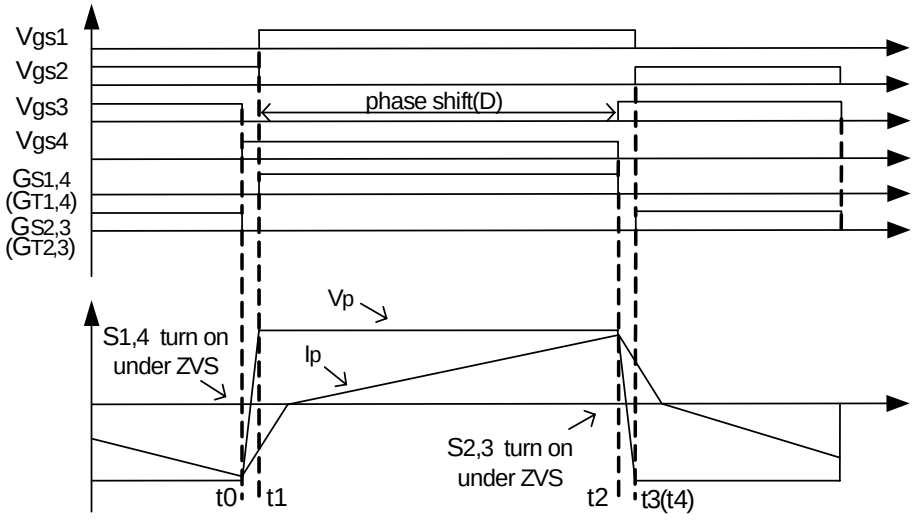

(b)

Fig. 2.2 Proposed soft switching scheme. (a) Light load condition. (b) Full load condition.

Fig. 2.2 shows the switching waveforms of converter operated by the proposed soft switching technique under light load condition and under full load condition. The duty ratio of switching signals (G_{S1-4}, G_{T1-4}) is not fixed at 50% but varies from 0% to 50% depending on the amount of phase shift (D), that is, the duty ratio of switching signal is D/2. The switch pairs, S_1, S_4 and S_2, S_3 in the diagonal position each turn on/off simultaneously. Therefore, there is no freewheeling interval in the proposed soft switching scheme, which reduces the circulating current, hence resulting in the reduction of conduction losses.

Since the positive half cycle is similar to the negative half cycle except that the signs of voltage and current are reversed, the analysis here of circuit operation is focused on the positive half cycle only. The circuit operations under light load and under full load are explained separately based on Fig. 2.2 (a), (b), where V_{gs1-4} are switching signals of S_{1-4} of the conventional switching scheme and G_{S1-4} and G_{T1-4} each are switching signals of S_{1-4} and T_{1-4} of the proposed switching scheme.

2.2.1 Circuit operation under light load

Mode I ($t_0<t<t_1$): All switches are off-state prior to t_0 and the primary current of the transformer, I_P, is zero. The switches, S_1 and S_4, are turned on under ZCS and the switches of the rectifier, T_1 and T_4, are also turned on under ZCS. The input voltage V_I begins to be applied to the transformer (Fig. 2.3 (a)).

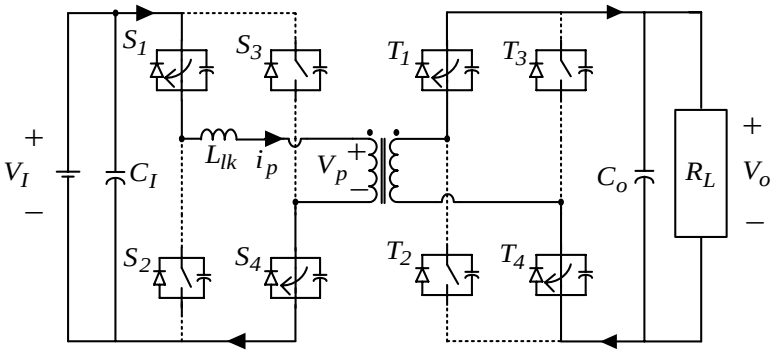

(a)

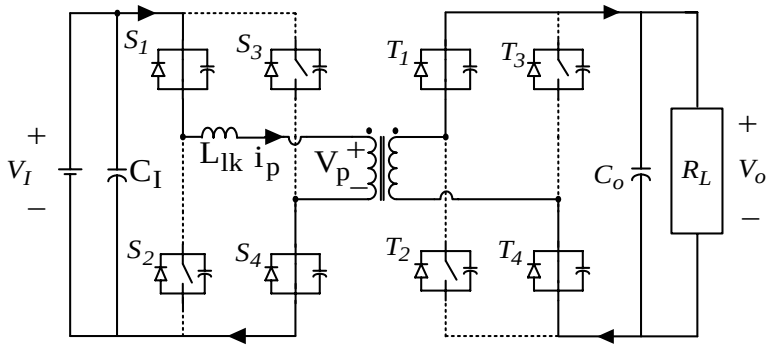

(b)

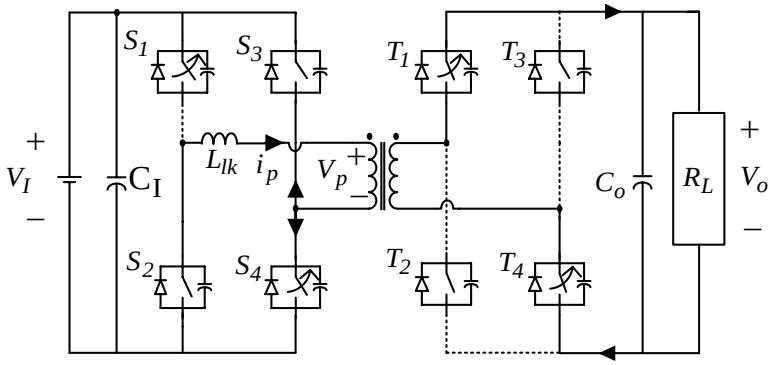

(c)

Fig. 2.3 Circuit operations under light load. (a) Mode I. (b) Mode II. (c) Mode III. (d) Mode IV.

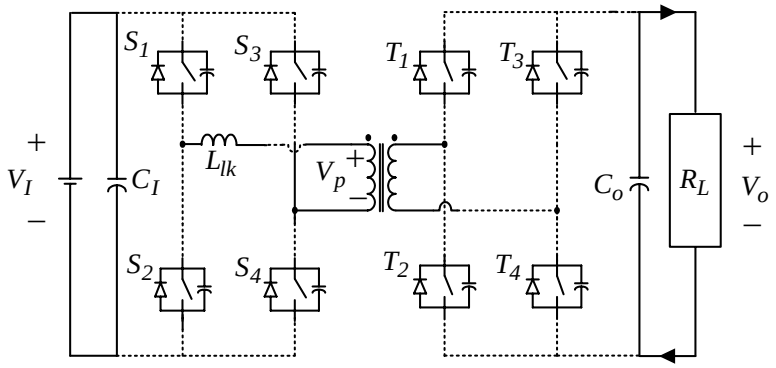

(d)

Fig. 2.3 Continued.

Mode II ($t_1<t<t_2$): The switches, S_1 and S_4, are on-state and the primary current, I_P, begins to increase and charge the leakage inductance of the transformer, L_{lk}. The power is transferred in the forward direction during this interval (Fig. 2.3 (b)).

Mode IV ($t_4<t<t_5$): All switches are off-state and the primary current reduces to zero at t_4. The output voltage, Vo, is kept constant by output capacitor. The switches, S_2 and S_3, will be turned on under ZCS during next negative half cycle (Fig. 2.3 (d)).

2.2.2. Circuit operation under full load

As the load increases, the primary current, I_P, increases and is not zero at the switching transition any more, and the switching operation begins to lose ZCS.

Mode I ($t_0<t<t_1$): The switches, S_2 and S_3, are on-state prior to t_0, and the primary current, I_P, is not zero which results in lose of ZCS at the switching of S_1 and S_4.

However, the primary current, I_P is big enough to discharge the capacitors, C_1 and C_4 and charge C_2 and C_3 for ZVS. The switches, S_2 and S_3, are turned off, and the primary current, I_P, discharges the capacitors, C_1 and C_4 and charges C_2 and C_3. After the voltages across C_1 and C_4 drop to zero, the body diodes, D_1 and D_4, conduct. Subsequently, the switches, S_1 and S_4, are turned on under ZVS (Fig. 2.4 (a)).

Mode II ($t_1<t<t_2$): The switches, S_1 and S_4, are on-state, and the primary current, I_P, in reverse direction reduces to zero and then increases in the forward direction. The power is transferred in the forward direction during this interval (Fig. 2.4 (b)).

Mode III ($t_2<t<t_3$): The switches, S_1 and S_4, are turned off, and the primary current, I_P, is sufficient for ZVS as in Mode I. The primary current discharges the capacitors, C_2 and C_3 and charges C_1 and C_4. After the capacitors, C_2 and C_3 are discharged completely, the body diodes, D_2 and D_3, conduct and subsequently the switches, S_2 and S_3 are turned on under ZVS (Fig. 2.4 (c)).

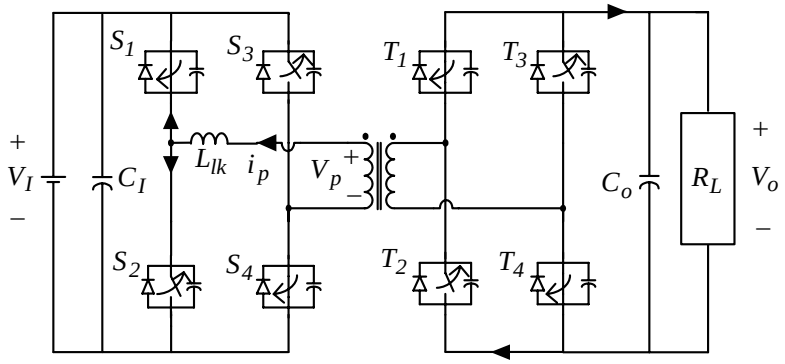

(a)

Fig. 2.4 Circuit operations under full load. (a) Mode I. (b) Mode II. (c) Mode III.

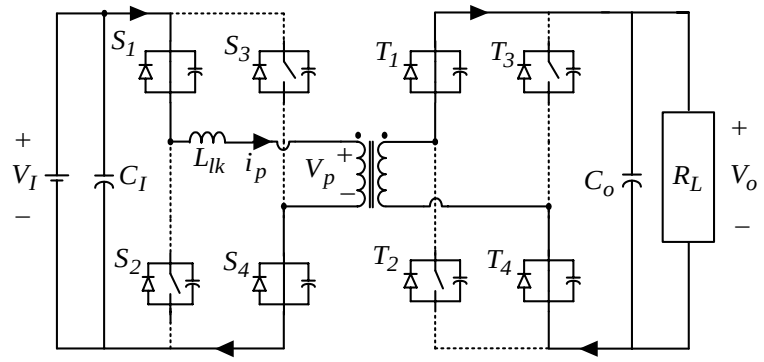

(b)

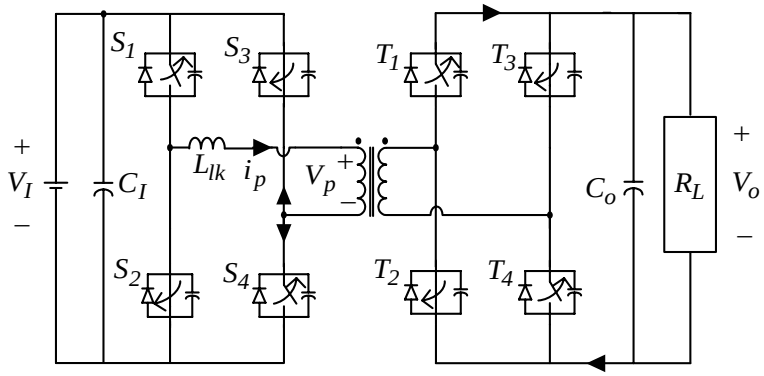

(c)

Fig. 2.4 Continued.

2.3 Load range for soft switching

In order to calculate the load range for soft switching, the minimum phase shift, D_{min}, for ZVS and the maximum phase shift, D_{max}, for ZCS are calculated. This is done because the phase shift amount is a function of the load, and the fact that all switches of this converter are turned on/off under soft switching from no load to full load is proven mathematically.

2.3.1 Maximum phase shift, D_{max}, for ZCS

At first, the on-mode is analyzed, where the switches, S_1 and $S_{4,}$ are on-state and the power is transferred in the forward direction. Then the off-mode is analyzed, where all switches are off-state after the switches, S_1 and $S_{4,}$ are turned off and the primary current, I_P, is not zero, both based on the circuit operation under light load condition assuming that the output capacitor, C_o, is sufficiently large to hold V_o at constant.

On-mode ($t_1<t<t_2$): The equivalent circuit of the converter referenced at the primary side during on-mode is shown in Fig. 2.5.

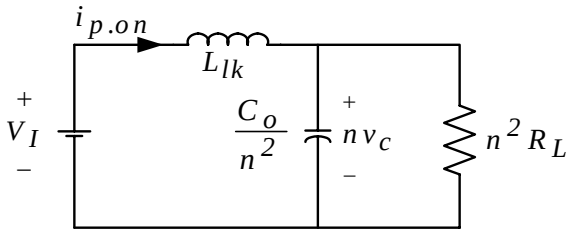

Fig. 2.5 Equivalent circuit of converter during on-mode.

The following equations are obtained using KVL and KCL;

$$VI = Llk\frac{d}{dt}(ip.on(t)) + nvc(t) \tag{2.1}$$

$$ip.on(t) = \frac{Co}{n}\frac{d(vc(t))}{dt} + \frac{vc(t)}{nR_L}, \tag{2.2}$$

where $n = N_1/N_2$, turn ratio of transformer.

Solving (2.1) and (2.2) using Laplace transform, and $i_{p.on}(t)$ is obtained after simplification assuming that $4n^2R_L{}^2Co >> Llk$, $2n^2R_L{}^2Co^2 >> Llk$ and $2R_LCo << 1$.

$$i_{p.on}(t) = \frac{V_I - nV_o}{Z_o}\sin(\omega_o t), \tag{2.3}$$

where $\omega_o = \frac{n}{\sqrt{L_{lk}C_o}}$ and $Z_o = n\sqrt{\frac{L_{lk}}{C_o}}$

and the peak primary current of transformer at t=DT/2= t_2-t_1 is

$$I_{peak} = i_{p,on}(D\frac{T}{2}) = D\pi\frac{\omega_o}{\omega_s}\frac{V_I - nV_o}{Z_o}, \tag{2.4}$$

where $T=1/f_s$ [19]

Off-mode ($t_3<t<t_4$): Fig. 2.6 shows the equivalent circuit referenced at the primary side during off-mode.

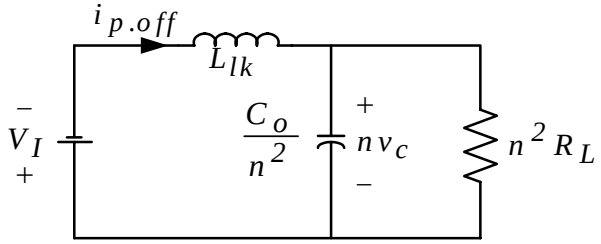

Fig. 2.6 Equivalent circuit of converter during off-mode.

The equations obtained are as follows;

$$V_I + L_{lk}\frac{d}{dt}(i_{p.off}(t)) + nv_c(t) = 0 \tag{2.5}$$

$$i_{p.off}(t) = \frac{C_o}{n}\frac{dv_c(t)}{dt} + \frac{v_c(t)}{nR_L} \tag{2.6}$$

Solving (3.5), (3.6), and $i_{p.off}(t)$ is obtained after simplification as on-mode.

$$ip,off\,(t) = Ipeak - \left(\frac{VI + nVo}{Zo} - \frac{Ipeak}{2nR_L}\sqrt{\frac{Llk}{Co}} \right)\sin(\omega ot) \qquad (2.7)$$

Since the primary current, $i_{p.off}(d_{off}T/2) = 0$ where $t=d_{off}T/2= t_4-t_3$., the peak value of primary current, $I_{peak,}$ can be obtained using (2.7).

$$Ipeak = \frac{\frac{VI + nVo}{Zo}\frac{\omega o}{\omega s}\pi doff}{1 + \frac{Zo}{2n^2 R_L}\frac{\omega o}{\omega s}\pi doff} \qquad (2.8)$$

Using (2.4) and (2.8), d_{off} is calculated.

$$doff \approx \frac{D(VI - nVo)}{VI + nVo} \qquad (2.9)$$

In order to get ZCS, the primary current should be zero prior to the next half cycle.

$$D\max\frac{T}{2} + doff\,\frac{T}{2} = \frac{T}{2}$$

$$D\max + doff = 1 \qquad (2.10)$$

Substituting (2.9) into (2.10), the maximum phase shift for ZCS, D_{max}, is obtained.

$$D\max = \frac{VI + nVo}{2VI} \qquad (2.11)$$

2.3.2 Minimum phase shift, D_{min}, for ZVS

Assuming lossless circuit elements, we get

$$\frac{1}{2}L_{lk}I_p^2 = \frac{1}{2}(C_1 + C_2 + C_3 + C_4)V_I^2$$

From energy balance consideration, and the minimum primary current to flow through the leakage inductance, L_{lk}, for ZVS is calculated as

$$I_p = 2V_I\sqrt{\frac{C_p}{L_{lk}}}, \tag{2.12}$$

where $C_P = C_{1\text{-}4}$.

Using (2.4) and (2.12), the minimum phase shift for ZVS is obtained.

$$D_{\min} = \frac{4V_I f_s\sqrt{C_p L_{lk}}}{V_I - nV_o} \tag{2.13}$$

From (2.11) and (2.13), we can get to conclusion that

$$D_{\max} > D_{\min} \tag{2.14}$$

because the parasitic values such as the leakage inductance of transformer, L_{lk}, and the parasitic capacitances of MOSFET, C_P, are trivial in the industrial applications. Considering that the maximum phase shift for ZCS is larger than minimum phase shift for ZVS and that the phase shift is a function of the load, we see that the proposed soft switching technique realizes the complete load range for soft switching from no load to full load without additional hardware components.

2.4 Experimental results and analysis

A low profile high frequency transformer, planar transformer, was employed as a link, and a prototype converter was built with design parameter specifications as Table 2.1.

Table 2.1 Design parameters.

V_I [V]	V_o [V]	f_s [kHz]	S_{1-4}	T_{1-4}	C_o [uF]	C_I [uF]	C_{1-4} [nF]	n N_1:N_2	L_{lk} [nH]
48	24	250	IRFP054N	IRFP054N	15	5	3.2	3:2	100

Fig. 2.7 shows the experimental switching waveforms where the load is 320W and the phase shift, D, is 0.75. The switches, S_2 and S_4 are turned on under ZCS (Fig. 2.7 (a)), while the switch S_2 loses ZVS under this light load (Fig. 2.7 (b)). The oscillation on the primary current waveform is due to resonances between the leakage inductance of transformer and the output capacitance of switch.

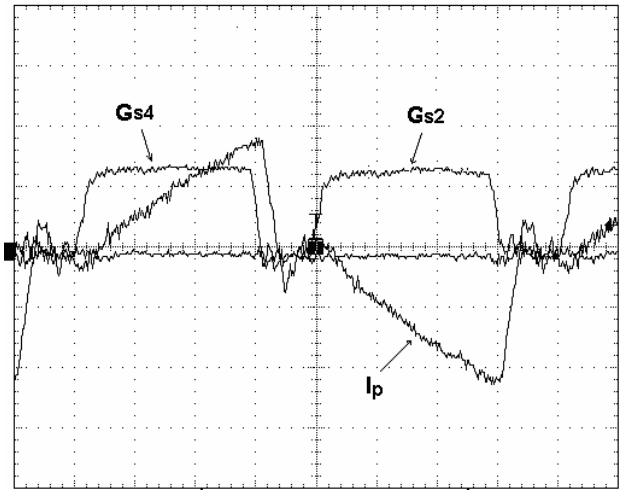

(a)

Fig. 2.7 Switching waveforms under light load. (a) ZCS switching waveforms of S_2 and S_4. (b) Non-ZVS switching waveforms of S_2 (V_{ds2}: Drain to source voltage of S_2, 25V/div, $G_{S2,4}$: Switching signals of $S_{2,4}$, 10V/div, I_P: Primary current, 5A/div).

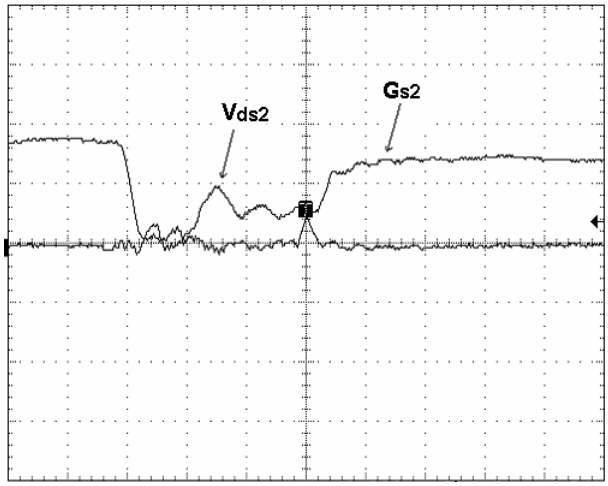

(b)

Fig. 2.7 Continued.

The drain to source voltage of S_2, V_{ds2}, should be $V_I/2$ during the interval that the switch S_1 and S_2 both are turned off under light load, but the primary current, I_P, discharges the capacitor C_2 right after S_1 is turned off and V_{ds2} reduces to the voltage less than $V_I/2$ (Fig. 2.7 (b)). As the load increases, the switch, S_4, begins to lose ZCS where the load is 440 W and D is 0.95 as shown in Fig. 2.8 (a). However, the primary current, I_P, is sufficient to discharge the capacitors, C_2 and C_4, and the switches, S_2 and S_4, are turned on under ZVS under full load (Fig. 2.8 (b),(c)), which indicates that the proposed switching technique realizes the complete load range for soft switching. As described above, this dc-dc converter consists of two active full–bridge converters with bi-directional power flow capability.

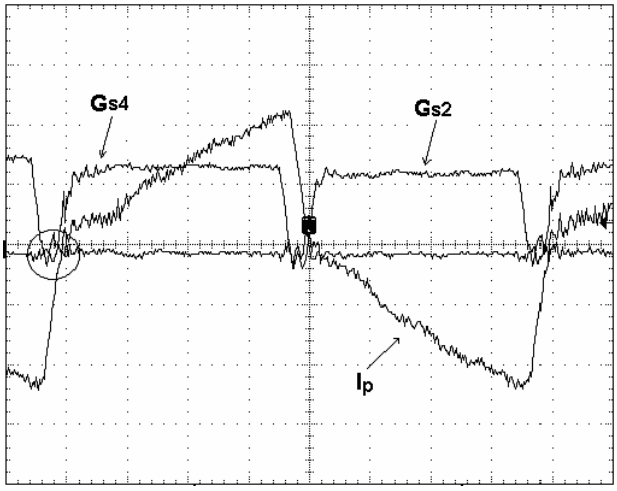

(a)

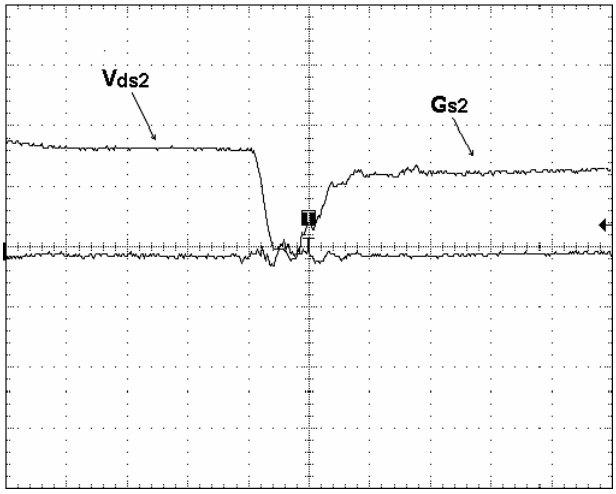

(b)

Fig. 2.8 Switching waveforms under full load. (a) Non-ZCS switching waveforms of S_2 and S_4, (b) ZVS switching waveforms of S_2. (c) ZVS switching waveforms of S_4 ($V_{ds2,4}$: Drain to source voltage of $S_{2,4}$, 25V/div, $G_{S2,4}$: Switching signals of $S_{2,4}$, 10V/div, I_P: Primary current, 5A/div).

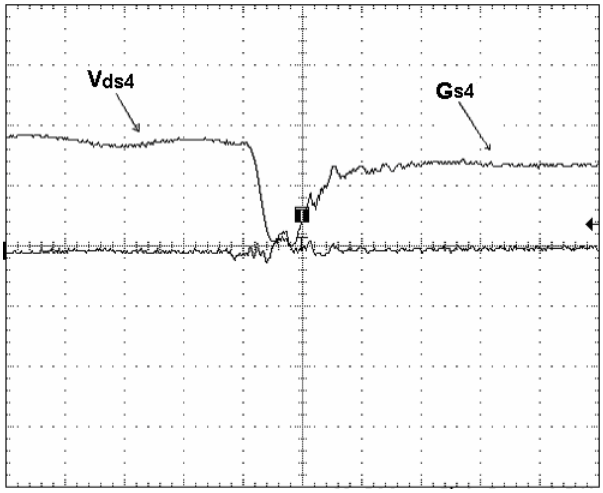

(c)

Fig. 2.8 Continued.

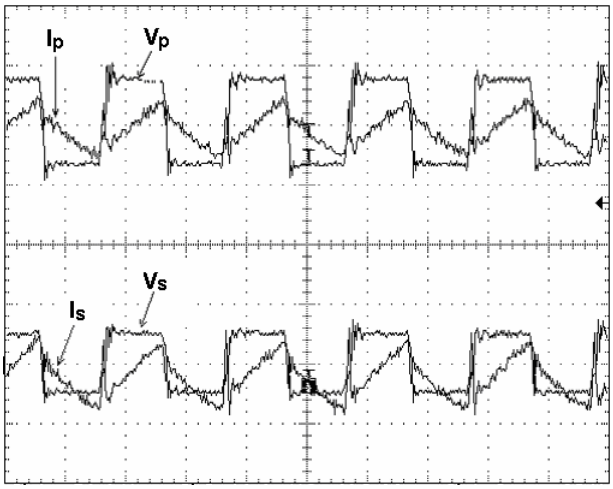

(a)

Fig. 2.9 Bi-directional power flow. (a) Forward power flow mode. (b) Reverse power flow mode (V_P: Primary voltage of transformer, 50V/div, I_P: Primary current, 5A/div, V_S: Secondary voltage of transformer, 50V/div, I_S: Primary current, 5A/div).

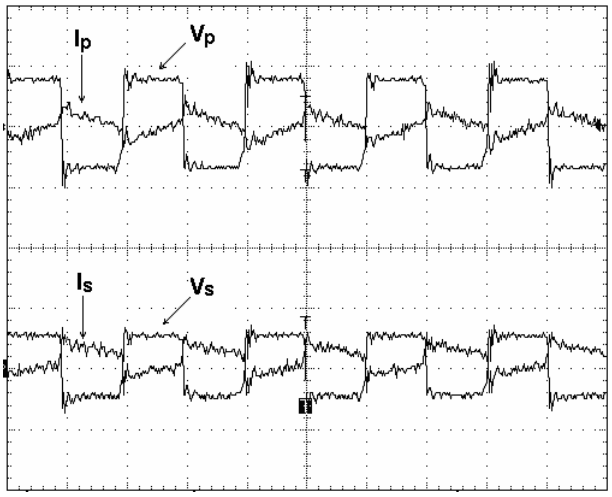

(b)

Fig. 2.9 Continued.

Fig. 2.9 shows the bi-directional power flow of converter. In reverse power flow mode where the external voltage source higher than the output voltage is connected to the load terminal (Fig. 2.9 (b)), the polarity of the primary current and the secondary current is opposite to the one of the primary voltage and the secondary voltage, which indicates the power flow from the secondary to the primary. The overall efficiency of converter is 90% which is primary degraded by the losses on the stray components of circuit and by the on-losses on the body diodes of MOSFETs on the secondary sides.

2.5 Conclusion

The bidirectional power flow, full-bridge dc-dc converter is a viable candidate for the buck/boost converter to charge a battery or supercapacitor during reverse power flow by regenerative breaking, which has attractive features in terms of low device

stress, small filter components, low switching losses and simple first order dynamics. In this chapter, a new soft switching technique using variable switching duty ratio for the bi-directional power flow full-bridge dc-dc converter was proposed. The proposed technique has been shown to achieve soft switching operation over wide load range. The proposed soft switching technique is also applicable to unidirectional dc-dc converter consisting of a full-bridge converter on the primary side and a diode rectifier and output filter on the secondary side.

CHAPTER III

A HIGH FREQUENCY LINK DIRECT DC-AC CONVERTER FOR RESIDENTIAL FUEL CELL POWER SYSTEMS

3.1 Introduction

Fuel cell has been considered as one of the highly promising alternatives for environmentally friendly renewable energy generation due to its high efficiency, modularity, and cleanness. One of its applications for medium power is the residential power system, where a compact dc-ac converter with galvanic isolation is required [20-23].

The high frequency (HF) link power conversion technique is attractive for this application because a bulky 60Hz transformer can be replaced with a compact high frequency transformer, and a high frequency link direct dc-ac converter which consists of a high frequency inverter, a cycloconverter, and a high frequency transformer between them, presents a possible way to build a compact direct dc-ac converter without the dc link capacitor and provides high conversion efficiency due to the reduced conversion step [12-13, 24].

Since the dc voltage generated by a fuel cell stack varies widely and is low in magnitude (36V to 60V), a front-end step-up dc-dc conversion stage is required to provide a regulated higher dc voltage to the high frequency link direct dc-ac converter. Due to the nature of the fuel supply process, the fuel cell response time to changes in power demand is slow and varies from few seconds to few minutes. Therefore, it is

necessary to improve the dynamics of the system by introducing the auxiliary power source [25]. In addition, it is crucial to reduce the low frequency current harmonics drawn from the fuel cell by high frequency link dc-ac converter because the varying reactant conditions surrounding the cells due to the low frequency current ripple may impose a severe impact to the performance of the fuel cell [26]. The dominant harmonic of the low frequency current harmonics drawn from the fuel cell is a 120Hz harmonic by a single phase high frequency link dc-ac converter whose output frequency is 60Hz, and the limit of 120Hz current harmonic is specified as 0.15 per-unit (i.e. 15% of its rated current) from 10% to 100% load in [27]. The low frequency voltage ripple at the dc bus caused by the substantial low frequency current ripple and a conventional sinusoidal PWM technique assuming a ripple-free dc voltage are the primary contributors for the appearance of low order harmonics in the high frequency link dc-ac converter output not present in the PWM switching functions, and are responsible for the deterioration in the quality of output voltage. A simple straightforward solution to this problem is to increase the output filter capacitance of the step-up dc-ac conversion stage, which makes it bulky and contributes to slow response, increased cost and losses [28].

In order to overcome these problems, a boost converter connected in series high frequency link direct dc-ac converter is proposed in this paper. A new multi-loop control to reduce the low frequency current harmonics drawn from the fuel cell and a new sinusoidal PWM technique for the cycloconverter at the secondary to reject the low order harmonics in the output voltage caused by the low frequency input voltage ripple are presented with proposed topology. The proposed multi-loop control reduces the

120Hz input current ripple of the boost converter dramatically without additional filter requirement, and the proposed PWM technique guarantees the high quality of the ac output voltage.

The performance of the proposed schemes is verified by the various simulation and experiment results, and their trade-offs are described in detail using mathematical evaluation approach.

3.2. Proposed high frequency link dc-ac converter

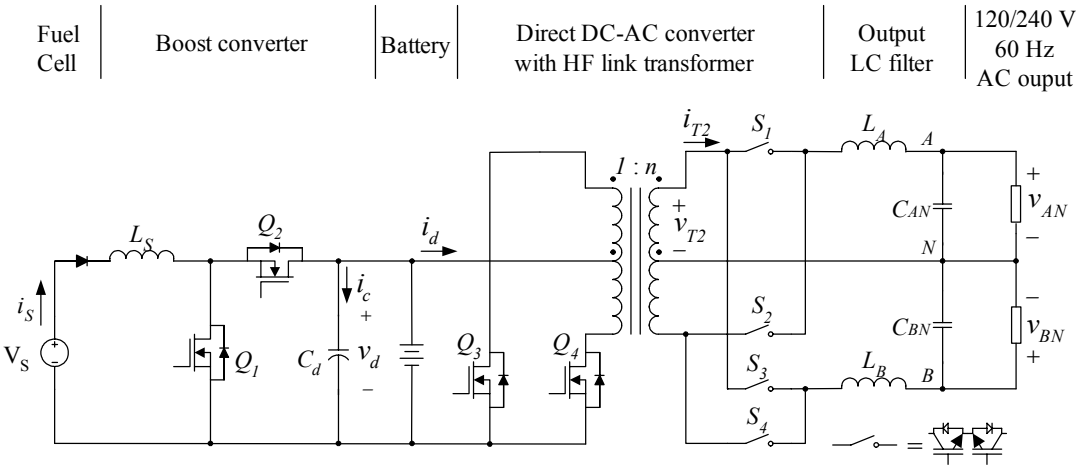

Fig. 3.1 Proposed high frequency link dc-ac converter.

Fig. 3.1 shows the proposed boost converter cascaded high frequency link dc-ac converter for residential fuel cell power system applications. Since the fuel cell terminal voltage varies significantly depending on the load change, it is required to boost and regulate the fuel cell voltage. The high frequency link transformer needs to be designed

to accommodate the lowest magnitude of the fuel cell voltage. During the normal operation the nominal input voltages are typically much higher than the minimum value and the transformer does not operate optimally [25]. Therefore, the boost converter step-up the fuel cell voltage to 84V, regulates and supplies a constant dc voltage to the input terminal of high frequency inverter at the primary, which allows the inverter to operate with a fixed duty ratio and does transformer to operate optimally. A battery pack is connected to the dc bus to provide fast system dynamic response. The high frequency inverter in push-pull connection at the primary generates a rectangular voltage waveform with 50% duty ratio and provides it to the secondary side through high frequency link transformer. The cycloconverter with a new PWM technique produces sinusoidally modulated 60Hz split single phase output voltage waveforms with high quality.

3.3 Multi-loop control for boost converter

The main propose of the front-end boost converter is to step-up the fuel cell voltage and regulate the output voltage and the input current. The magnitude of the low frequency (120Hz) input current ripple is highly dependent on the voltage control loop characteristic and the size of capacitor, C_d, at the dc bus.

The output voltage and current of high frequency link dc-ac converter are defined simply as follows

$$vo(t) = \sqrt{2}Vo.rms \sin(\omega ot)$$

$$io(t) = \sqrt{2}Io.rms \sin(\omega ot - \phi), \tag{3.1}$$

where ϕ is power factor angle.

The instantaneous output power, $P_o(t)$, is

$$Po(t) = vo(t)io(t)$$
$$= Vo.rmsIo.rms\cos\phi - Vo.rmsIo.rms\cos(2\omega ot - \phi)$$

Considering power balance with assumption that $v_d(t)$ is a constant dc value, V_d, the dc current $i_d(t)$ is

$$id(t) = Id + id.rppl(t)$$
$$= \frac{Vo.rmsIo.rms}{Vd}\cos\phi - \frac{Vo.rmsIo.rms}{Vd}\cos(2\omega ot - \phi) \quad (3.2)$$

$$ic(t) = -id.rppl(t)\,, \quad (3.3)$$

where 120Hz ripple current as large as fundamental current is included in the current of dc bus terminal. The dc bus voltage with a voltage ripple caused by the 120 Hz current ripple across C_d is expressed as follows

$$vd(t) = Vd + \frac{1}{Cd}\int ic(t)dt = Vd(1 + k\sin(2\omega ot - \phi))\,,$$

where $k = \dfrac{Vo.rmsIo.rms}{2\omega oCdVd^2}$ (3.4)

The steady state voltage error calculated in the voltage control loop of boost converter becomes

$$verr(t) = Vd - vd(t) = -\frac{Vo.rmsIo.rms}{2\omega oCdVd}\sin(2\omega ot - \phi)\,, \quad (3.5)$$

and the current reference of the current loop is the voltage error multiplied by voltage loop gain. Therefore, a large 120Hz ripple current which is 180º phase shifted from the 120Hz ripple voltage at the dc bus is induced at the fuel cell terminal with a conventional PI control, and deteriorates the performance of fuel cell power system. In

order to reduce the 120Hz input ripple current, a new multi-loop control is proposed (Fig. 3.2). An additional control loop with gain K_c is added to the PI voltage control loop, and the voltage error multiplied by K_c cancels the 120Hz ripple component of the current reference of the current control loop and eliminates the 120Hz input ripple current at the fuel cell terminal. A limiter on the current reference limits the sudden large current reference command during start up or load change and prevents the inductor from saturating and does the switching devices from being damaged.

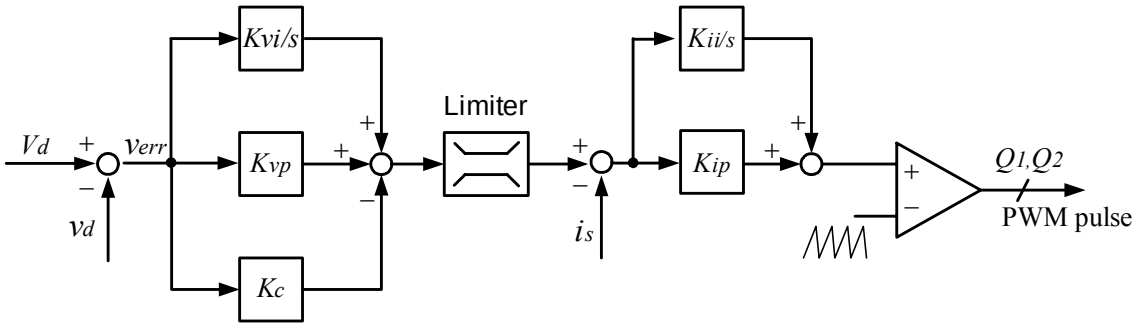

Fig. 3.2 Block diagram of proposed multi-loop control.

Fig. 3.3 shows the simulation results obtained with 10% voltage ripple at the output of boost converter. The input current ripple with the proposed multi-control scheme is reduced from $i_{s.pp}$=27.2 to $i_{s.pp}$=3.8A, and the 120Hz harmonic of input current is reduced from $I_{s.h2}$=0.3p.u. to $I_{s.h2}$=0.008p.u., while the output voltage ripple, $v_{d.pp}$, is increased by 2.1%. The increased voltage ripple at the dc bus is counted into designing a new PWM scheme for the cycloconverter at the secondary. During load transition, the maximum overshoot of v_d is increased by multi-loop control, but its effect is mitigated

by the battery in parallel with C_d and the independent voltage control with a new PWM technique for the cycloconverter.

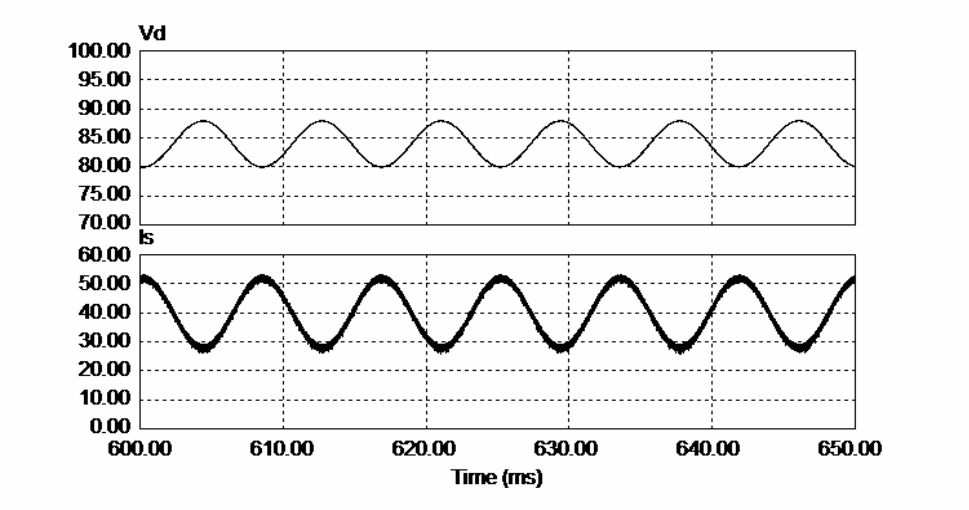

(a)

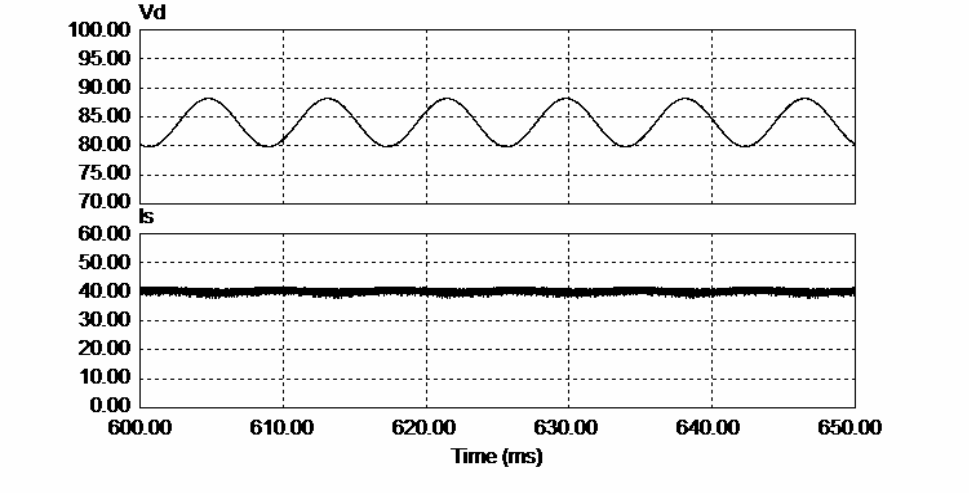

(b)

Fig. 3.3 Waveforms of i_s and v_d. (a) v_d and i_s with conventional PI control. (b) v_d and i_s with proposed multi-loop control (f_{sw} = 40kHz, L_s = 60uH, C_d = 5.5mF and P_o=1.5kVA).

3.4 Proposed PWM technique for cycloconverter

In this section, the performance of the proposed PWM technique for the cycloconverter at the secondary is analyzed using a switching function approach. The PWM switching signals of cycloconverter are obtained by converting the level of the PWM switching signals of the single phase inverter composed of unidirectional switches according to the polarity of the ac link voltage. The PWM switching signals of cycloconverter are same as those of single phase inverter when the polarity of ac link voltage is positive. On the other hand, when the polarity of ac link voltage is negative, the PWM switching signals of cycloconverter are generated by reversing the level of PWM switching signals of the inverter [6]. Therefore, the PWM switching functions and output voltages of the cycloconverter can be expressed in the same manner as those of single phase inverter using Fourier series. The switching functions can be written as

$$\begin{bmatrix} Sa(t) \\ Sb(t) \end{bmatrix} = \begin{bmatrix} \sum_{m=1}^{\infty} Am \sin m(\omega ot) \\ \sum_{m=1}^{\infty} Am \sin m(\omega ot - \pi) \end{bmatrix} \tag{3.6}$$

For the ripple-free dc bus voltage, V_d, the respective output voltages are given by

$$vAN(t) = nVdSa(t) = nVd \sum_{m=1}^{\infty} Am \sin m(\omega ot)$$

$$vBN(t) = nVdSb(t) = nVd \sum_{m=1}^{\infty} Am \sin m(\omega ot - \pi),$$

where n is transformer turn ratio. (3.7)

However, the dc bus voltage of single phase high frequency link dc-ac converter has 120Hz voltage ripple caused by the inherent 120Hz input current ripple as mentioned

in the third section. The output voltages with 120Hz voltage ripple at the dc bus can be written as follows using (3.4) and (3.6)

$$v_{AN}(t) = nvd(t)Sa(t) = nVd \sum_{m=1}^{\infty} Am \sin m(\omega ot) + \frac{nVdk}{2} \sum_{m=1}^{\infty} Am(\cos(2\omega ot - \phi - m\omega ot) - \cos(2\omega ot - \phi + m\omega ot))$$

$$v_{BN}(t) = nvd(t)Sb(t) = nVd \sum_{m=1}^{\infty} Am(\sin m(\omega ot - \pi) + \frac{nVdk}{2} \sum_{m=1}^{\infty} Am(\cos(2\omega ot - \phi - m(\omega ot - \pi)) - \cos(2\omega ot - \phi + m(\omega ot - \pi))) \quad (3.8)$$

It is apparent that low order harmonics at ($2\omega_o t - \phi \pm m\ \omega_o t$) and ($2\omega_o t - \phi \pm m(\omega_o t - \pi)$), not present in the PWM switching functions, appear in the output voltages due to the dc-link voltage ripple.

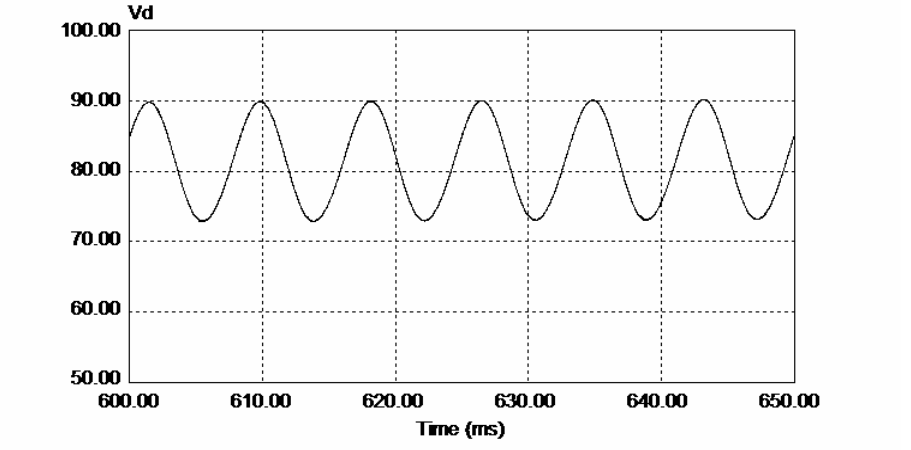

(a)

Fig. 3.4 Output voltage waveforms with conventional PWM technique. (a) v_d with 20% ripple. (b) v_{AN} and v_{BN}. (c) Frequency spectrum of v_{AN} (f_{sw}=20kHz and modulation index, m_a= 0.7).

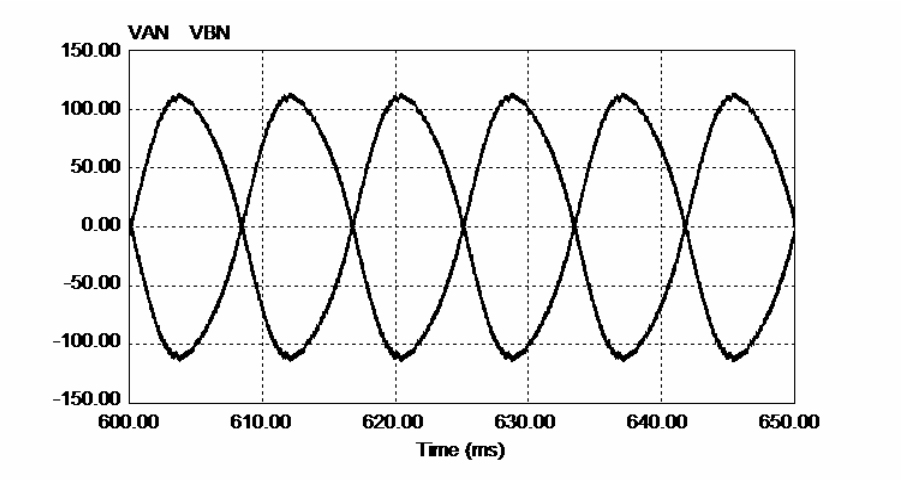

(b)

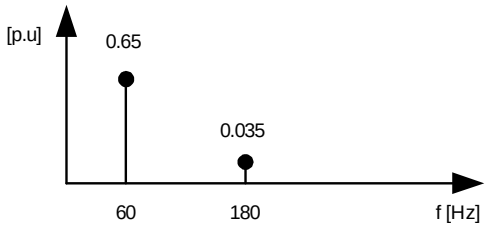

(c)

Fig. 3.4 Continued.

The simulation is carried out with 120 Hz voltage ripple of 20% (i.e., k=0.1) in the dc bus. Fig. 3.4 illustrates that the conventional PWM technique with 120Hz voltage ripple in the dc bus generates the 3rd harmonics in the output voltages and distorts the output waveforms.

3.4.1 Proposed PWM technique to cancel the low order harmonics

In order to eliminate the low order harmonics in the output voltages caused by the conventional PWM switching functions, (3.6), with 120Hz voltage ripple in the dc bus, new PWM switching functions are proposed as follows

$$\begin{bmatrix} Sa.new(t) \\ Sb.new(t) \end{bmatrix} = \frac{1}{1 + k\sin(2\omega ot - \phi)} \begin{bmatrix} \sum_{m=1}^{\infty} Am \sin m(\omega ot) \\ \sum_{m=1}^{\infty} Am \sin m(\omega ot - \pi) \end{bmatrix} \tag{3.9}$$

The respective output voltages then become

$$vAN(t) = nvd(t)Sa.new(t) = nVd \sum_{m=1}^{\infty} Am \sin m(\omega ot)$$

$$vBN(t) = nvd(t)Sb.new(t) = nVd \sum_{m=1}^{\infty} Am \sin m(\omega ot - \pi) \tag{3.10}$$

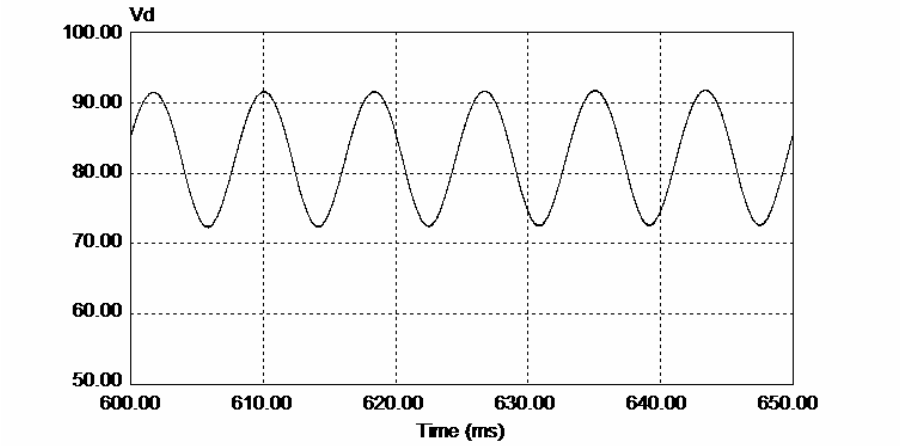

(a)

Fig. 3.5 Output voltage waveforms with proposed PWM technique. (a) v_d. (b) Modified modulation index, m_a. (c) v_{AN} and v_{BN}. (d) Frequency spectrum of v_{AN}.

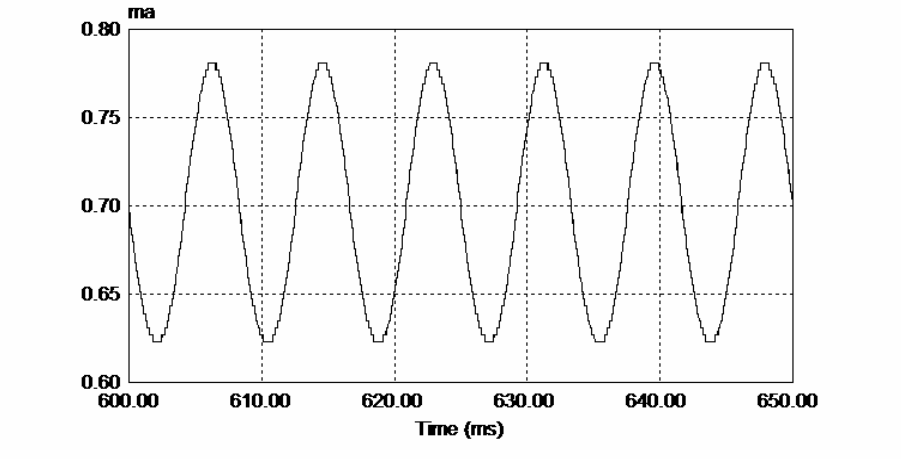

(b)

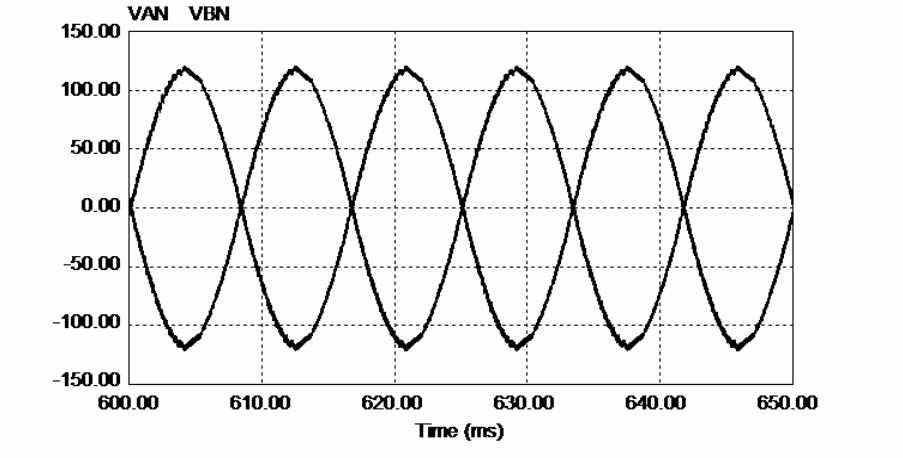

(c)

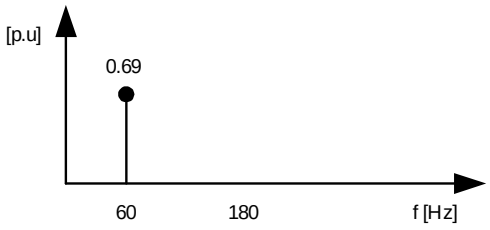

(d)

Fig. 3.5 Continued.

Equation (3.10) is identical to (3.7) where the 120Hz voltage ripple is zero. Therefore, the proposed PWM technique cancels the low order harmonics in the output voltages without increasing the filter capacitor (C_d), and guarantees the output voltages with high quality. Fig. 3.5 shows the simulation results obtained with proposed PWM switching functions, where the PWM technique is implemented by changing the modulation index according to the voltage ripple adaptively (Fig. 3.5 (b)). Fig. 3.5 (d) illustrates the frequency spectrum of output voltage and depicts the cancellation of low order harmonics.

3.4.2 Evaluation of proposed PWM technique

(a) Current ripple in the dc bus: The dc current, $i_d(t)$, in the dc bus with proposed switching technique is given by

$$id(t) = n(Sa.new(t)iAN(t) + Sb.new(t)iBN(t)) \tag{3.11}$$

The magnitude of dc component and the low order harmonics can be obtained using a geometric series. The simplified dc term and the low order harmonics are given by

$$Id = nI(A1 + \frac{A1k^2}{2}) \tag{3.12}$$

$$Ih2 = -nI((A1 + \frac{A1k^2}{4})\cos 2\omega ot + (A1k + \frac{3A1k^3}{4})\sin 2\omega ot) \tag{3.13}$$

$$Ih4 = -nI(\frac{A1k^2}{2}\cos 4\omega ot - (\frac{A1k}{2} + \frac{3A1k^3}{8})\sin 4\omega ot)\ , \tag{3.14}$$

where I is a peak value of each phase current and m=1.

Fig. 3.6 shows the frequency spectrum of dc current, i_d, with 20% voltage ripple at the dc bus. For a modulation index m_a=0.7 (i.e., $A_1=m_a/2$=0.35), I_{h2}=0.36 p.u. at 120Hz and I_{h4}=0.036 p.u. at 240Hz. Thus, it can be concluded that the proposed PWM technique effectively eliminates the low order harmonics of the output voltages, but the dc current of the dc bus, i_d, will be distorted by the increased I_{h2} and I_{h4}. For reasonable magnitude of voltage ripple at the dc bus, the magnitudes of I_{h2} and I_{h4} are not high.

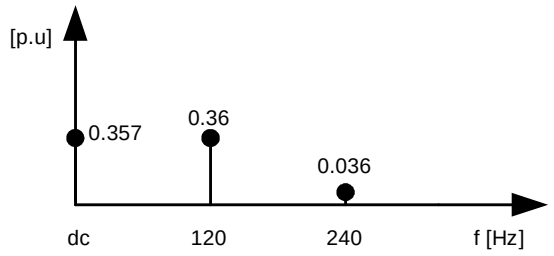

Fig. 3.6 Frequency spectrum of i_d.

(b) Voltage gain of high frequency link dc-ac converter: The 120Hz voltage ripple of the dc bus (Fig. 3.5 (a)) also appears in the ac link voltage at the secondary with an amplitude multiplied by the transformer turn ratio (*n*), and reduces the margin to incorporate higher instantaneous values of the modulating signal given by the proposed switching functions (3.9). Moreover, this insufficient margin is proportional to the magnitude of voltage ripple. Thus, there is an upper limit to which the modulation index can be raised with proposed switching functions for a particular magnitude of voltage ripple, which results in losses of voltage gain. Therefore, considering the increased

voltage ripples by the multi-loop control and the increased I_{h2} and I_{h4} resulted from the proposed PWM technique, Δk_1 and Δk_2 each, the percentage voltage gain of high frequency link dc-ac converter with voltage ripple of magnitude k is given by

$$Gv = (1-(k+\Delta k1+\Delta k2))\times 100\% \tag{3.15}$$

The reduced voltage gain at 20% voltage ripple is 11.5% in Fig. 3.7.

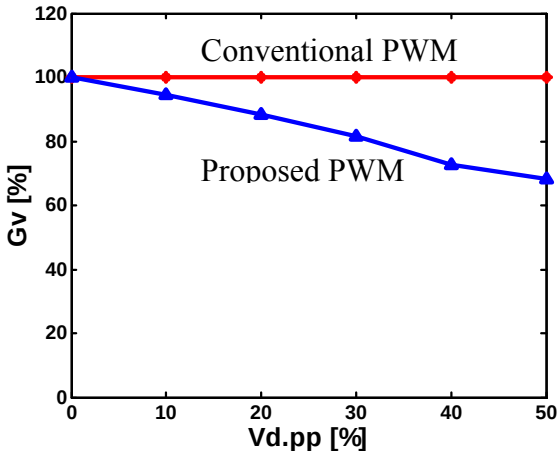

Fig. 3.7 Voltage gain versus $V_{d.pp.}$

(c) Output voltage quality: Fig. 3.8 presents the total harmonic distortion (THD) of the output voltage (v_{AN}) at various percentage of dc voltage ripple, both with a conventional PWM technique and with the proposed PWM technique. For 50% voltage ripple, the total increased voltage ripple by the multi-loop control and the proposed PWM technique is 63.4% (i.e., $k+\Delta k_1+\Delta k_2$=0.32) at the modulation index, m_a=0.7, where the margin to incorporate higher instantaneous values of the modulating signal is insufficient and the THD of output voltage is increased to 11.6%.

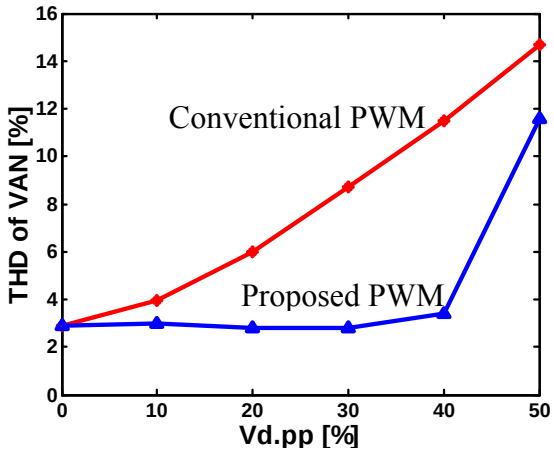

Fig. 3.8 THD of output voltage (v_{AN}).

Thus, the margin of modulating signal should be larger than the total voltage ripple of the dc bus to avoid a severe distortion of output voltage.

$$1 - ma \geq k + \Delta k1 + \Delta k2 \tag{3.16}$$

3.4.3 Calculation of C_d

The required capacitance of C_d for a desired voltage ripple ($2kV_d$) is calculated using the equation (3.4) as follows

$$Cd = \frac{Po}{(k - (\Delta k1 + \Delta k2))2\omega o Vd^2} \tag{3.17}$$

In addition, the capacitance of C_d also satisfies the following equation for the proper operation of the boost converter.

$$Cd = \frac{Is.pkLs}{2kVd(Vd - Vs)} \tag{3.18}$$

3.5 Generation of switching sequence

3.5.1 Switching sequence

The switching sequence of the proposed dc-ac converter is shown in Fig. 3.9. In this figure, bidirectional switches in phase A and B are shown to explain how to obtain split single-phase sinusoidal ac output voltages. The PWM control is carried out by switching signals generated by DSP board where a sawtooth waveform carrier having twice of the ac link frequency and control signals V_a^* and V_b^* are compared. The switching sequence of the bidirectional switches is determined as follows. The switches, Q3 and Q4, of the inverter at the primary are turned on and off synchronized with the edge of the sawtooth carrier signal. Therefore, the ac link voltage, V_{T2}, has rectangular waveform with 50% duty ratio.

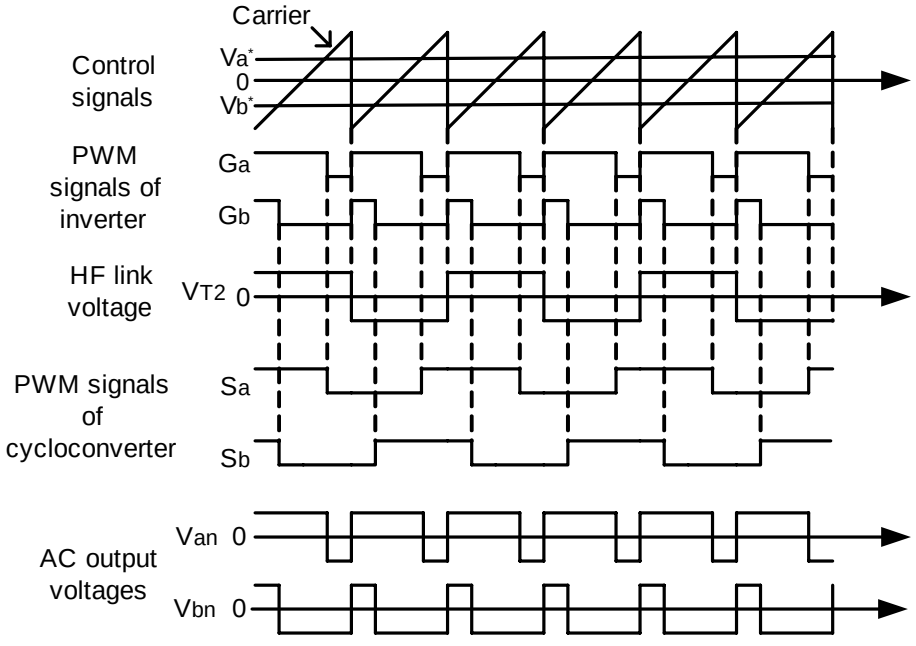

Fig. 3.9 Switching sequence.

The PWM switching signals of cycloconverter at the secondary, S_a and S_b, are obtained by converting the level of the PWM switching signals of the single phase inverter composed of unidirectional switches, G_a and G_b, according to the polarity of the ac link voltage. The PWM switching signals of cycloconverter are same as those of single phase inverter when the polarity of ac link voltage is positive. On the other hand, when the polarity of ac link voltage is negative, the PWM switching signals of cycloconverter are generated by reversing the level of PWM switching signals of the inverter [6].

3.5.2 4-step switching strategy

The cycloconverter at the secondary has difficulties to commutate inductive load current from one bidirectional switch to another due to finite switch on/off times. Since the instantaneous switching is practically impossible, the on/off operation of a semiconductor switch requires a finite delay time. If an overlap between the switching is provided, the source side voltage essentially short-circuited. A finite amount of switching delay is therefore mandatory. This, however, results in the interruption of inductive load current causing damaging voltage spikes on the switches. Therefore, lossy snubber circuits are required to protect the switching device from voltage spikes. The proposed 4-step strategy independently controls each switching device of a bidirectional switch depending on the input voltage or load current polarity. This approach offers safe transition of inductive load current at all power factor from one bidirectional switch to

another and ensures safe switching operation even in the presence of source side stray inductance. [29-30]

With an inductive load, a cycle of input can be divided into 4 modes according to the direction of input voltage and load current as followings (Fig. 3.10).

Mode 1: $V_I > 0$, $i_L > 0$

Mode 2: $V_I > 0$, $i_L < 0$

Mode 3: $V_I < 0$, $i_L > 0$

Mode 4: $V_I < 0$, $i_L < 0$

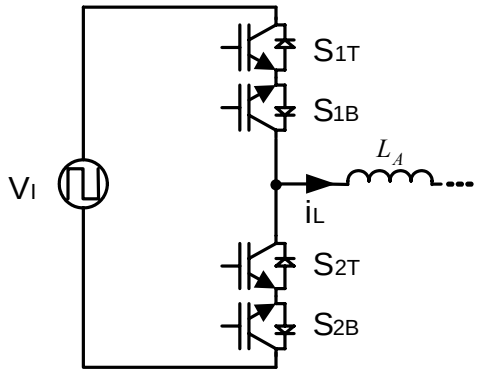

Fig. 3.10 Simplified cycloconverter circuit of phase A.

The operation of 4 step switching sequence is divided into voltage and current reference mode according to the reference signal. Voltage reference mode uses input voltage polarity as a reference, and current reference mode uses load current polarity as a reference. The brief explanation of each mode of operation is following.

A. Voltage reference mode

In this mode, input voltage polarity is used as a reference signal. Therefore, switching sequences of mode 1 and mode 2 are identical, since their input voltage polarity is same. Similarly, mode 3 and mode 4 use same switching sequence. The operation sequences for commutation from S_{1T} and S_{1B} to S_{2T} and S_{2B} are described as follows.

In the case of commutation from S_{2T} and S_{2B} to S_{1T} and S_{1B}, the 4 step switching will follow exactly reverse sequence of the above. The example of the gate signals for voltage reference mode operation is shown in Fig. 3.11, where V_P represent reference signal, that is input voltage polarity, and V_{CS} represents switch conduction state.

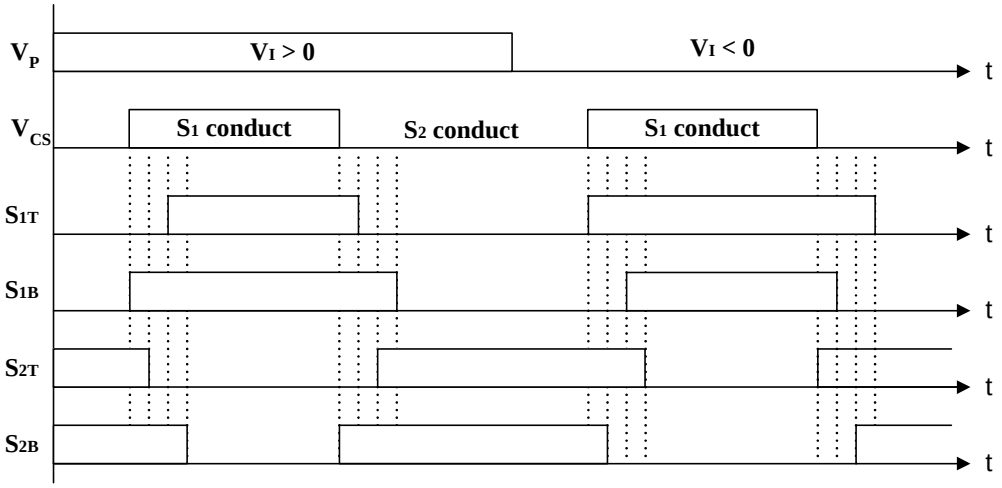

Fig. 3.11 Voltage reference mode 4-step switching signals.

Mode 1: $V_I>0$ and $i_L>0$ (S_{1T} is conducting)

Step1: turn on S_{2B} – Nothing happen since S_{2B} is reverse biased.

Step2: turn off S_{1T} – The load current is transferred from S_{1T} to $S_{2B.}$

Step3: turn on S_{2T} – Nothing happen.

Step4: turn off S_{1B} – S_1 is turned off

Mode 2: $V_I>0$ and $i_L<0$ (S_{1B} is conducting)

Step1: turn on S_{2B} – Nothing happen since S_{2B} is reverse biased.

Step2: turn off S_{1T} – Nothing happen.

Step3: turn on S_{2T} – The load current is transferred from S_{1B} to $S_{2T.}$

Step4: turn off S_{1B} – S_1 is turned off.

Mode 3: $V_I<0$ and $i_L>0$ (S_{1T} is conducting)

Step1: turn on S_{2T} – Nothing happen since S_{2T} is reverse biased.

Step2: turn off S_{1B} – Nothing happen.

Step3: turn on S_{2B} – The load current is transferred from S_{1T} to $S_{2B.}$

Step4: turn off S_{1B} – S_1 is turned off.

Mode 4: $V_I<0$ and $i_L<0$ (S_{1B} is conducting)

Step1: turn on S_{2T} – Nothing happen since S_{2T} is reverse biased.

Step2: turn off S_{1B} – The load current is transferred from S_{1B} to $S_{2T.}$

Step3: turn on S_{2B} – Nothing happen.

Step4: turn off S_{1B} – S_1 is turned off.

B. Current reference mode

The current reference mode operation is similar to voltage reference mode except the load current polarity is used as a reference signal. Therefore, switching sequences of mode 1 and mode 3 are identical, since their load current polarity is same. Similarly, mode 2 and mode 4 use same switching sequence. The operation sequences for commutation from S_{1T} and S_{1B} to S_{2T} and S_{2B} are described as follows. The example of the gate signals for current reference mode operation is shown in Fig. 3.12, where V_P represent reference signal, that is load current polarity, and V_{CS} represent switch conduction state.

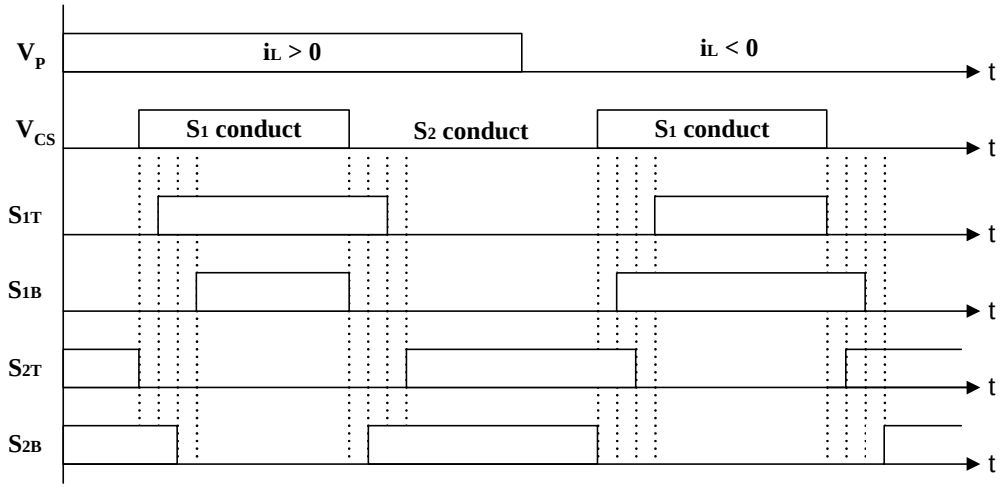

Fig. 3.12 Current reference mode 4-step switching signals.

Mode 1: $V_I>0$ and $i_L>0$ (S_{1T} is conducting)

Step1: turn off S_{1B} – Nothing happen.

Step2: turn on S_{2B} – Nothing happen since S_{2B} is reverse biased.

Step3: turn off S_{1T} – The load current is transferred from S_{1T} to $S_{2B.}$

Step4: turn on S_{2T} – S_2 is turned on.

Mode 2: $V_I>0$ and $i_L<0$ (S_{1B} is conducting)

Step1: turn off S_{1T} – Nothing happen.

Step2: turn on S_{2T} – The load current is transferred from S_{1B} to $S_{2T.}$

Step3: turn off S_{1B} – S_1 is turned off.

Step4: turn on S_{2B} – Nothing happen.

Mode 3: $V_I<0$ and $i_L>0$ (S_{1T} is conducting)

Step1: turn off S_{1B} – Nothing happen.

Step2: turn on S_{2B} – The load current is transferred from S_{1T} to S_{2B}.

Step3: turn off S_{1T} – S_1 is turned off.

Step4: turn on S_{2T} – Nothing happen.

Mode 4: $V_I<0$ and $i_L>0$ (S_{1B} is conducting)

Step1: turn off S_{1T} – Nothing happen.

Step2: turn on S_{2T} – Nothing happen since S_{2T} is reverse biased.

Step3: turn off S_{1B} – The load current is transferred from S_{1B} to $S_{2T.}$

Step4: turn on S_{2B} – Nothing happen.

C. 4 step switching technique for electronic transformer

The voltage reference mode is employed in order to apply 4-step switching technique into the cycloconverter. The polarity of input voltage is decided based on the

switching signal of Q3 of the inverter at the primary generated by DSP board, and 4-step switching sequence is implemented by a programmable controller, FPGA chip.

3.6 A three-phase high frequency link direct dc-ac converter

3.6.1 Analysis of three-phase high frequency link dc-ac converter

A three-phase high frequency link direct dc-ac converter is obtained with same topology using two switching functions having 60° difference in phase.

$$\begin{bmatrix} Sa(t) \\ Sb(t) \end{bmatrix} = \begin{bmatrix} \sum_{m=1}^{\infty} Am \sin m(\omega ot) \\ \sum_{m=1}^{\infty} Am \sin m(\omega ot - \frac{\pi}{3}) \end{bmatrix} \tag{3.19}$$

The three-phase output voltages are calculated in same manner as the case of single-phase system.

$$vac(t) = nVdSa(t) = nVd \sum_{m=1}^{\infty} Am \sin m(\omega ot)$$

$$vbc(t) = nVdSb(t) = nVd \sum_{m=1}^{\infty} Am \sin m(\omega ot - \frac{\pi}{3})$$

$$vab(t) = vac(t) - vbc(t) = nVd \sum_{m=1}^{\infty} Am \sin m(\omega ot + \frac{\pi}{3}), \tag{3.20}$$

where n is transformer turn ratio.

The dc current at dc bus, $i_d(t)$, is given by

$$id(t) = n(Sa(t)ia(t) + Sb(t)ib(t)) \tag{3.21}$$

The output voltage and current of three-phase dc-ac converter can be expressed in vector diagram as in Fig. 3.13, and their simulation waveforms are given in Fig. 3.14.

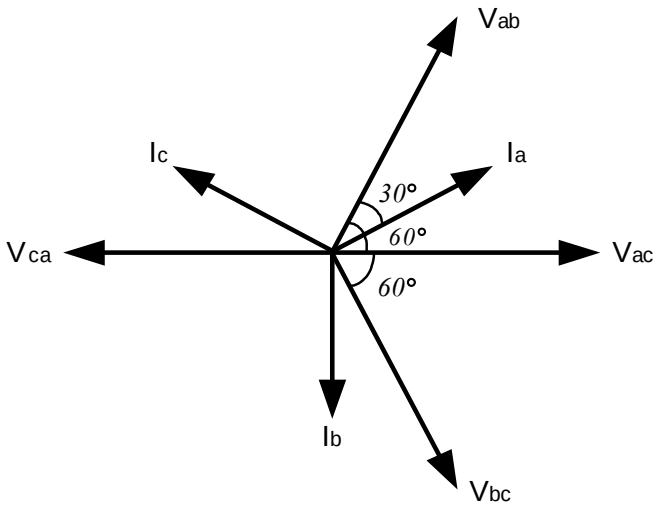

Fig. 3.13 Vector diagram of three-phase system.

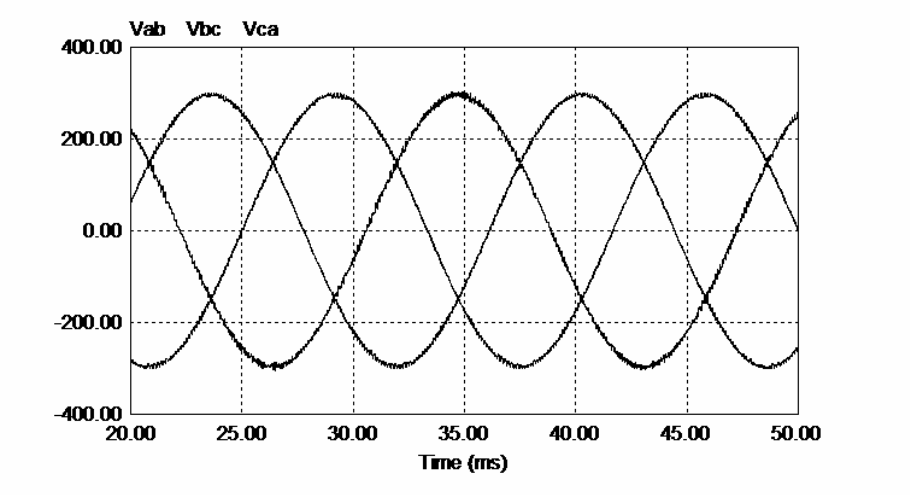

(a)

Fig. 3.14 Simulation results of three-phase dc-ac converter. (a) Output voltage waveform. (b) Output current waveforms.

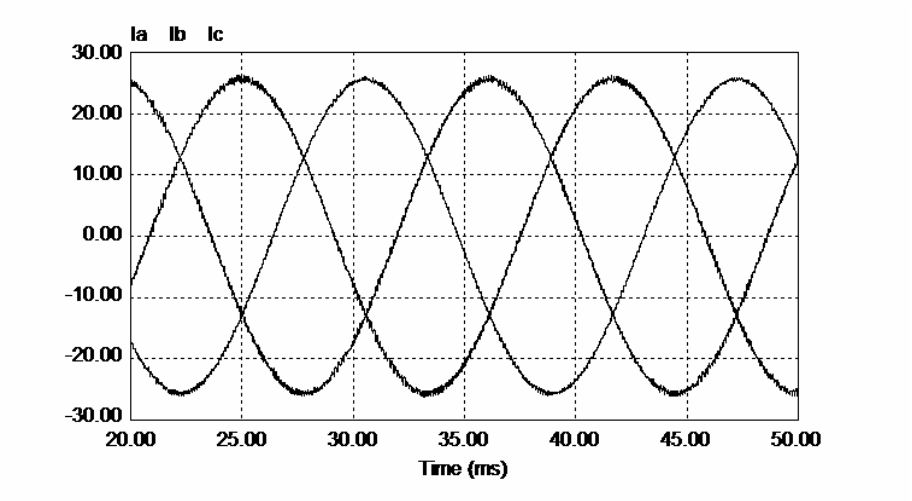

(b)

Fig. 3.14 Continued.

3.6.2 Comparative evaluation with a conventional high frequency three-phase direct dc-ac converter

The three-phase direct dc-ac converter (B4) is compared with a conventional three-phase direct dc-ac converter (B6) which has six bi-directional switches at the secondary based on the mathematically obtained rating data of a bi-directional switch and transformer. In Table 3.1, the transformer VA rating and the voltage rating and current rating of the bi-directional switch of the conventional three-phase direct dc-ac converter each are considered 1 per-unit. Table 3.1 shows that the VA rating of the bi-directional switch and transformer of the proposed direct dc-ac converter (B4) each are 1.48 times and 1.6 times larger than those of the conventional direct dc-ac converter (B6), which is resulted from the reduction of the bi-directional switch count from six to

four in the proposed topology, and that the turn ratio of the transformer is 0.8 times smaller than that of the conventional dc-ac converter.

Table 3.1 Component ratings of three-phase dc-ac converter.

	Voltage rating of switch, V_{SW}	Current rating of switch, A_{SW}	V·A rating of transformer, VA_{TR}	Turn ratio of transformer, N
B4	1.6 pu	0.93 pu	1.6 pu	0.8 N_1
B6	1 pu	1 pu	1 pu	N_1

3.7 Experimental results

In order to provide experimental verification of the proposed scheme, a boost converter cascaded high frequency link direct dc-ac converter has been built with TMS320LF2407 and FPGA chip, where the fuel cell voltage (36V) is converted to the 60Hz, 120V_{rms} split single-phase AC output voltages. The boost converter and dc-ac converter operate at 40kHz and at 20kHz each. The input inductor of boost converter is 60uH, and two values of output capacitor, C_d, 5.5mF for 10% voltage ripple and 3.3mF for 20% voltage ripple are used to verify the simulation results, which were properly designed using equations (3.17 and 3.18) for desired voltage ripples at the dc bus. Fig. 3.15 shows that the waveforms of the output voltage and input current obtained from the boost converter, and illustrates that the proposed multi-control scheme reduces the

120Hz input current ripple harmonic to the magnitude less than 10% of dc value, which improves the performance of fuel cell system.

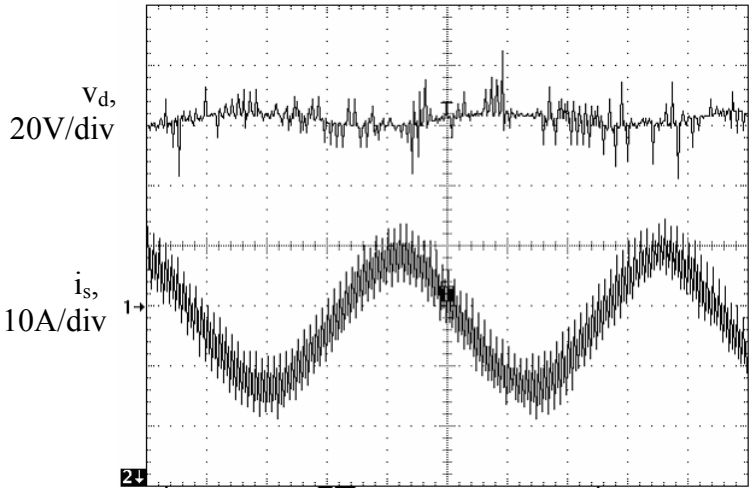

(a)

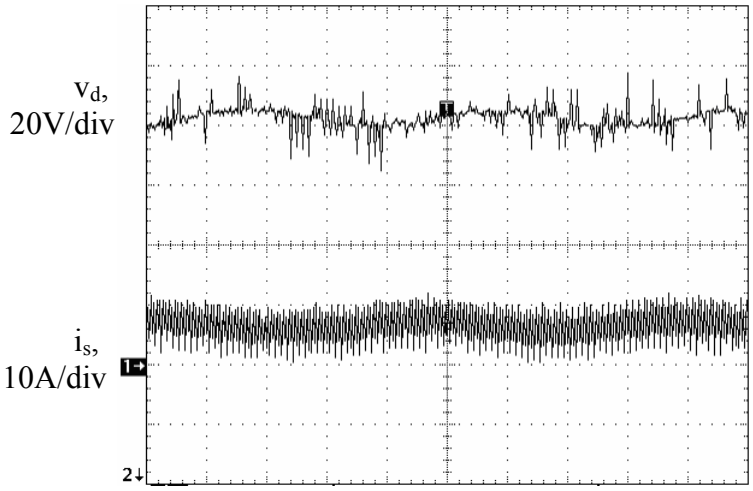

(b)

Fig. 3.15 Output waveforms of boost converter. (a) Conventional PI control. (b) Multi-loop control.

Fig. 3.16 shows that the voltage ripple at the dc bus with a conventional PWM technique assuming ripple-free voltage at the dc bus generates distorted output voltages with the 3rd harmonic at 180Hz.

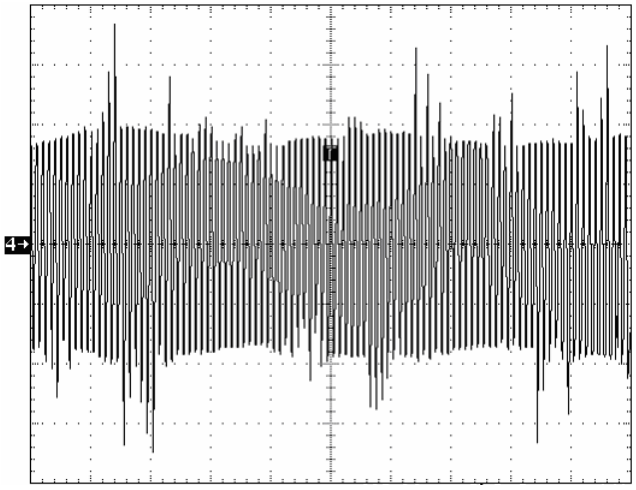

(a)

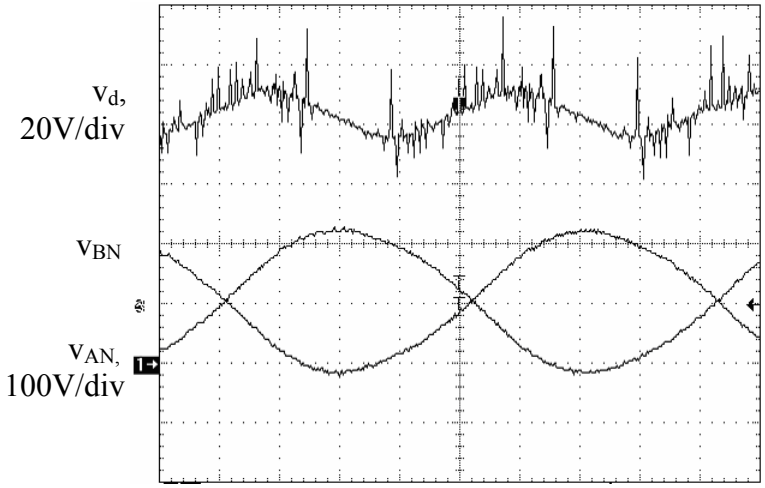

(b)

Fig. 3.16 Output voltage waveforms of dc-ac converter with a conventional PWM technique under 20% voltage ripple and m_a=0.7. (a) AC link voltage, v_{T2}, 100V/div. (b) Output voltage waveforms. (c) Frequency spectrum of v_{AN}, 20V_{rms}/div.

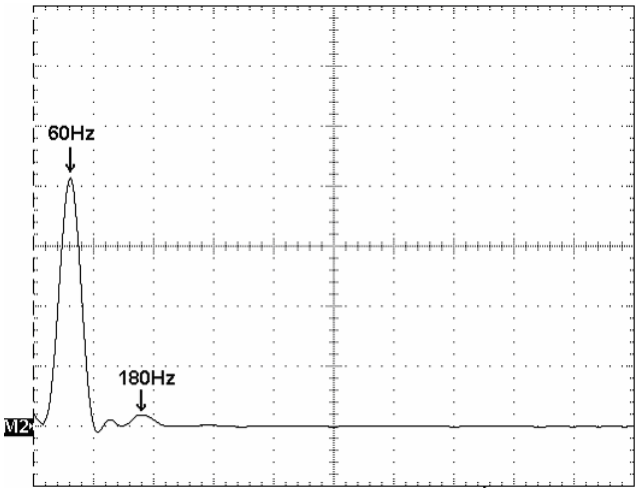

(c)

Fig. 3.16 Continued.

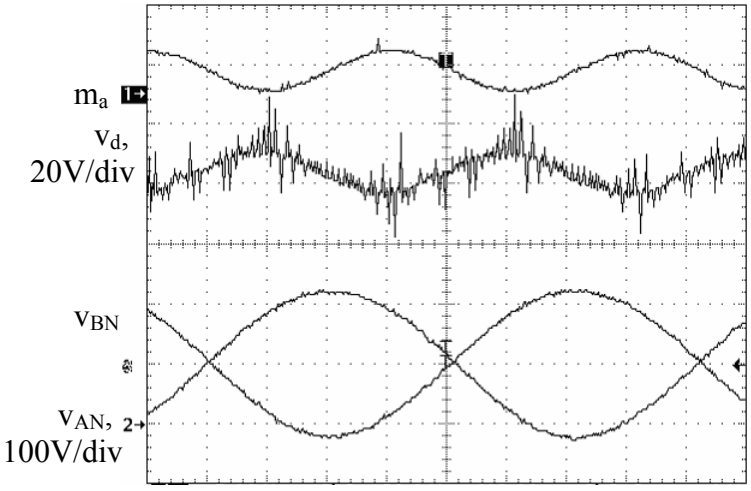

(a)

Fig. 3.17 Output voltage waveforms of dc-ac converter with a proposed PWM technique. (a) Output voltage waveforms. (b) Frequency spectrum of v_{AN}, 20V_{rms}/div.

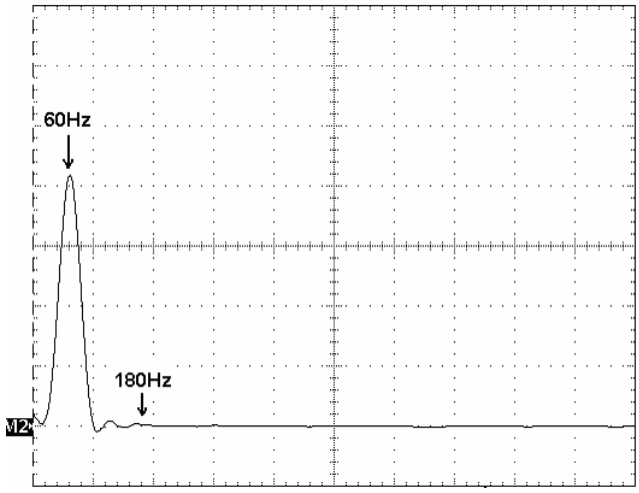

(b)

Fig. 3.17 Continued.

The proposed PWM technique is implemented by DSP, where an adaptive modulating signal is generated based on the sensed dc voltage ripple, and it eliminates the 3rd harmonic of output voltage effectively and produces the output voltage waveforms with high quality (Fig. 3.17).

3.8 Conclusion

In this chapter, a boost converter cascaded high frequency link direct dc-ac converter for fuel cell power sources has been proposed. The boost converter has been shown to regulate the dc bus voltage effectively when the fuel cell voltage varies widely depending on the load condition. Further, the proposed multi-loop control of the boost converter has been shown to reduce the 120Hz input current harmonic drawn from the fuel cell to less than 10% without additional filter requirements. The evaluation of

proposed PWM technique illustrates that immunity to voltage ripple at the dc bus can be achieved only at the expense of loss of voltage gain in the dc-ac converter and marginal dc current distortion. Experimental results have been shown to validate the feasibility of the proposed approach.

CHAPTER IV

A CURRENT-FED HIGH FREQUENCY LINK DIRECT DC-AC CONVERTER WITH ACTIVE HARMONIC FILTER FOR FUEL CELL POWER SYSTEMS

4.1 Introduction

The fuel cell has been considered as one of highly promising alternatives for environmentally friendly renewable energy generation due to its high efficiency, modularity, and cleanness. One of its applications for medium power is the residential power system, where a compact dc-ac converter with galvanic isolation is required [20-23].

The high frequency link power conversion technique is attractive for this application because a bulky 60Hz transformer can be replaced with a compact high frequency transformer, and a high frequency link direct dc-ac converter which consists of a high frequency inverter, a cycloconverter, and a high frequency transformer between them presents a possible way to build a compact direct dc-ac converter without the dc link capacitor, which provides the high conversion efficiency due to the reduced conversion step [12-13, 24, 34-35].

Since the residential power system needs the split single phase output voltages of $120V_{rms}$ from the low dc voltage source (36V to 60V), a boost type converter or a high turn ratio of the transformer is required [9]. The current-fed dc-ac converter is known as an effective solution for the power conversion from the low voltage to the high voltage because it can operate in the buck and boost modes, and provide easy balancing of

transformer [36-38]. Moreover, a current-fed converter requires less size of the input filter because the primary inductor is placed in the input side [22-23]. However, a large input filter is still required to cancel the low frequency current harmonics drawn from the fuel cell by high frequency link dc-ac converter because the varying reactant conditions surrounding the cells due to the low frequency current ripple may impose a severe impact to the performance and durability of the fuel cell [26]. The dominant harmonic of the low frequency current harmonic drawn from the fuel cell is a 120Hz harmonic by a single phase high frequency link dc-ac converter whose output frequency is 60Hz, and the limit of 120Hz current harmonic is specified as 0.15 per-unit (i.e. 15% of its rated current) from 10% to 100% load in [27].

In order to solve these problems, a current-fed high frequency link direct dc-ac converter with an active harmonic filter is proposed in this paper. The current-fed high frequency link direct dc-ac converter generates the split single phase ac outputs from the fuel cell powered dc source in a single power conversion stage. The active harmonic filter makes the compensation current eliminating the input harmonic current of 120 Hz drawn from the fuel cell using an electrolytic capacitor. In this summary, the operation and control of the proposed high frequency link dc-ac converter are presented in detail and the simulation results are provided to verify the usefulness of the proposed scheme.

4.2 Proposed current-fed high frequency link direct dc-ac converter

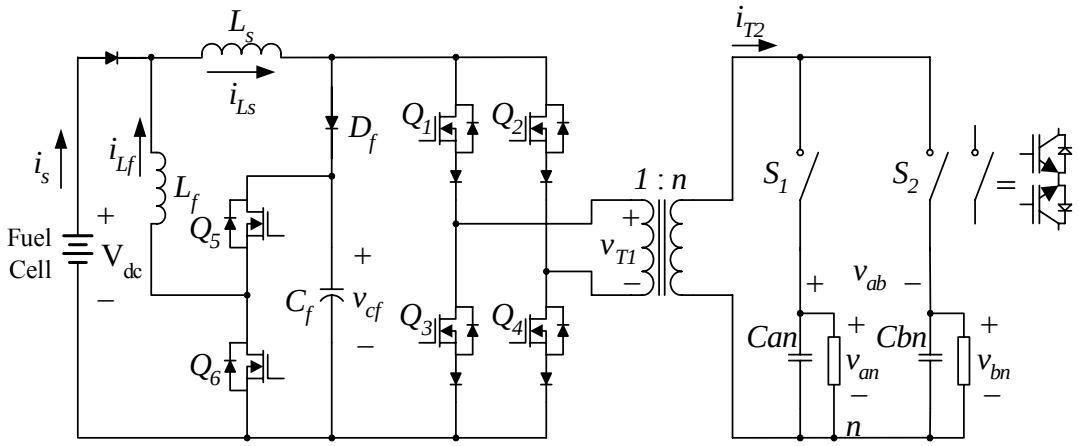

Fig. 4.1 Proposed current-fed high frequency link direct dc-ac converter.

Fig. 4.1 shows the proposed current-fed high frequency link direct dc-ac converter with an active harmonic filter for fuel cell applications. The current-fed high frequency full-bridge inverter at the primary that consists of an inductor (L_s) and four reverse-blocking MOSFET switches ($Q_{1\text{-}4}$) with diodes generates sinusoidally PWM modulated current pulses with zero current switching (ZCS) for two single phases each, and provides them to the secondary via high frequency link transformer. The cycloconverter at the secondary which consists of only two bidirectional switches($S_1$and S_2) and output filter capacitors (C_{an} and C_{bn}) produces sinusoidally modulated 60Hz split single phase output voltage waveforms(V_{an} and V_{bn}) with near zero current. The active harmonic filter makes the compensation current eliminating the harmonic current of 120 Hz that appears in the input side. The diode D_f and capacitor C_f in the active filter are used for the voltage clamping in the high frequency inverter operation without the

additional claming circuits. The proposed configuration offers a simple structure, easy balancing of the high frequency transformer and an effective solution to eliminating the 120 Hz input current ripple.

There are three operating modes in the proposed current-fed high frequency link direct dc-ac converter; the powering, reset, and restoring modes.

4.2.1 Powering mode

Two diagonal switches (Q_1 and Q_4, or Q_2 and Q_3) are closed under zero current in the powering mode as shown in Fig. 4.2.(a). The current i_{Ls} of the primary inductor is sinusoidally modulated separately for two single phases by the full-bridge inverter and transferred to the output through the high frequency transformer and cycloconverter. The bi-directional switch for each phase is closed with fixed duty ratio at the near zero current according to the polarities of the modulated link current and the desired output voltage.

4.2.2 Reset mode

Two upper or lower switches (Q_1 and Q_2, or Q_3 and Q_4), or all four switches are opened in the reset mode as shown in Fig. 4.2 (b). The inductor current i_{Ls} flows through the diode D_f and charges the capacitor C_f . The primary inductor is generally reset through a flyback winding in the conventional current-fed approaches [31-33], which has the complexity of the inductor and produces a high impact current. These disadvantages are easily overcome in the proposed scheme. The capacitor voltage v_{Cf} can

be controlled by the switches Q_5 and Q_6 during the active filter operation and is maintained to be higher than the input voltage V_{dc} and the transformer primary voltage v_{T1}.

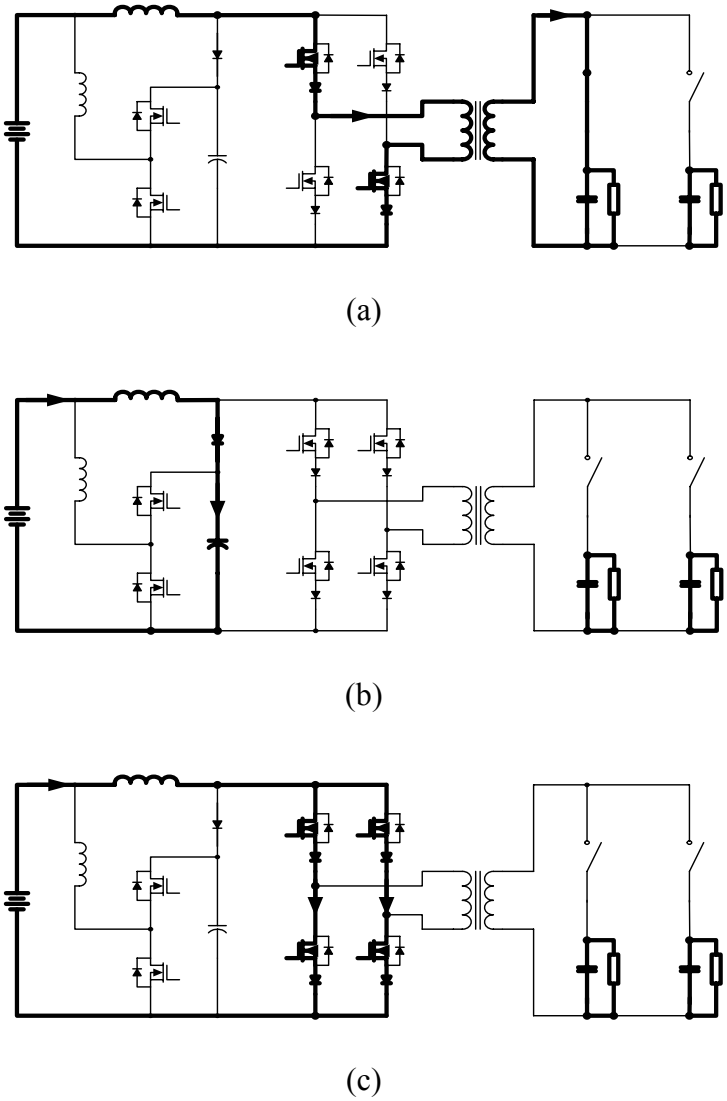

Fig. 4.2 Operating modes of current-fed high frequency link dc-ac converter. (a) Powering mode. (b) Reset mode. (c) Restoring mode.

4.2.3 Restoring mode

Both switches of one inverter leg (Q_1 and Q_3, or Q_2 and Q_4), or all four switches are closed under zero current as shown in Fig. 4.2 (c). Thus, the inductor current increases with a rate of V_{dc}/L_s in the restoring mode while decreases with a rate of (V_{dc}-v_{Cf})/L_s in the reset mode.

Therefore, the primary inductor current can be controlled by appropriate selection of the reset and restoring mode during the interval that the primary current is not transferred to the secondary side.

4.3 Active cancellation of 120Hz input harmonic current

The input and output powers of the inverter should be balanced in both average and instantaneous senses. The output voltage and current of the dc-ac converter with a sinusoidal output can be expressed simply as

$$vo(t) = \sqrt{2}Vrms\sin\omega ot \tag{4.1}$$

$$io(t) = \sqrt{2}Irms\sin(\omega ot - \phi)\,, \tag{4.2}$$

where ϕ denotes a power factor angle. The instantaneous power is derived from (4.1) and (4.2) as

$$Po(t) = vo(t)io(t) = VrsmIrms - VrmsIrms\cos(2\omega ot - \phi) \tag{4.3}$$

The average power is defined as

$$Pav = VrmsIrms\cos\phi \tag{4.4}$$

The input current for a constant input voltage of V_{dc} can be represented as

$$is(t) = \frac{VrmsIrms}{Vdc}\cos\phi - \frac{VrmsIrms}{Vdc}\cos(2\omega ot - \phi) \tag{4.5}$$

The second term of the right hand side in (4.5) is the second order ripple current defined as

$$ir(t) = -\frac{VrmsIrms}{Vdc}\cos(2\omega ot - \phi) \tag{4.6}$$

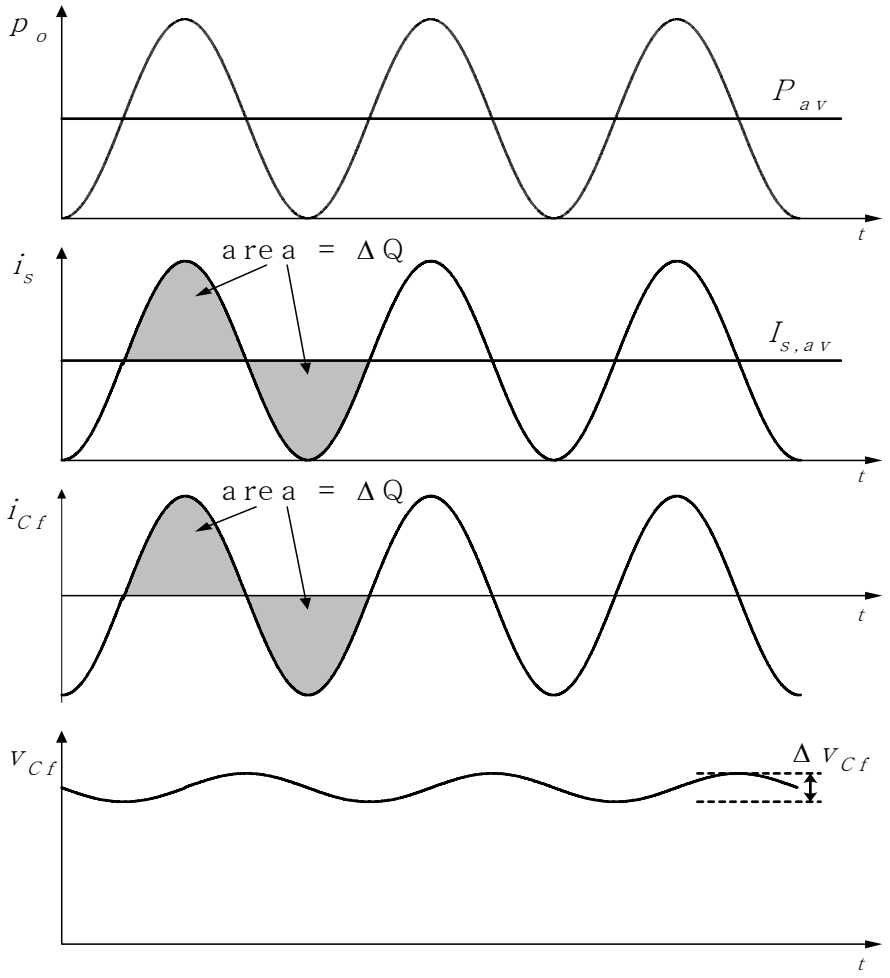

Fig. 4.3 Output power, input current, capacitor current and voltage waveforms.

The basic concept of the proposed technique is that the capacitor C_f stores the charge ΔQ from the DC source during the negative half cycle of the ripple current and then supplies the stored charge to the output during the positive half cycle. Fig. 4.3 shows the output power, input current, net capacitor current, and capacitor voltage. The charge ΔQ is equal to the area of the half cycle and can be represented as

$$\Delta Q = \sqrt{2} Irms / 60\pi \, . \tag{4.7}$$

The voltage ripple of the filter capacitor C_f can be calculated from (4.7) as

$$\Delta vcf = \Delta Q / Cf \, . \tag{4.8}$$

Fig. 4.4. shows the operation of the active harmonic filter, where it is assumed that the filter capacitor voltage v_{cf} is controlled to be higher than V_{dc} and v_{T1}.

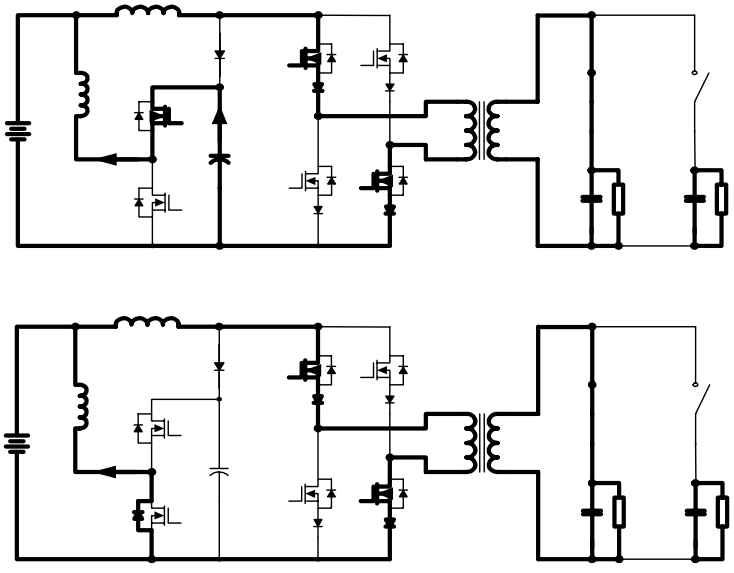

(a)

Fig. 4.4 Operating modes of active harmonic filter. (a) Buck mode. (b) Boost mode.

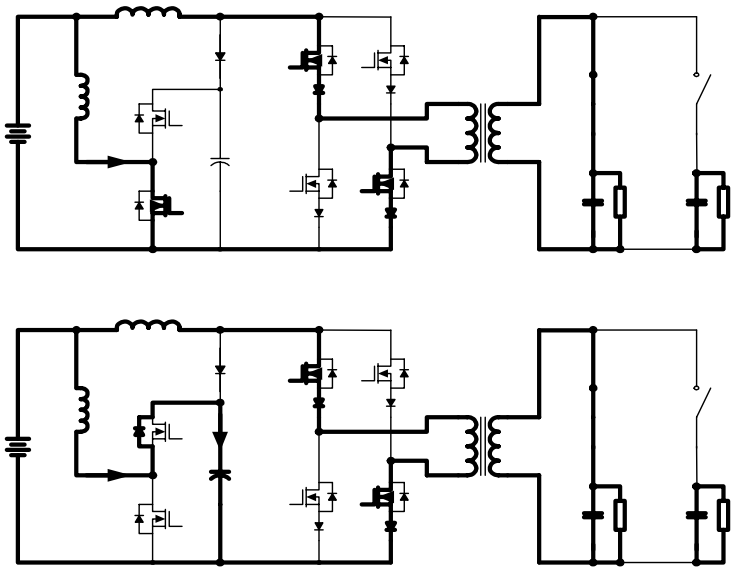

(b)

Fig. 4.4 Continued.

Two operating modes can be considered for the active filter operation. One is the buck mode as shown in Fig. 4.4 (a). The switch Q_5 and diode D_6 operates in this mode and the stored charge is supplied to the output through the filter inductor L_f. The other is the boost mode as shown in Fig. 4.4 (b). The current of the filter inductor flows from the source to the filter capacitor and the filter capacitor is charged by the boosting action of the switch Q_6 and diode D_5.

4.4 Control strategy

4.4.1 Control of output voltage

Fig. 4.5 (a) shows the voltage control scheme for the main high frequency link dc-ac converter. The output voltage is controlled by the PWM of the full-bridge inverter, where G_v(s) is the gain of the voltage control loop. A simple proportional (P) control is used for G_v(s).

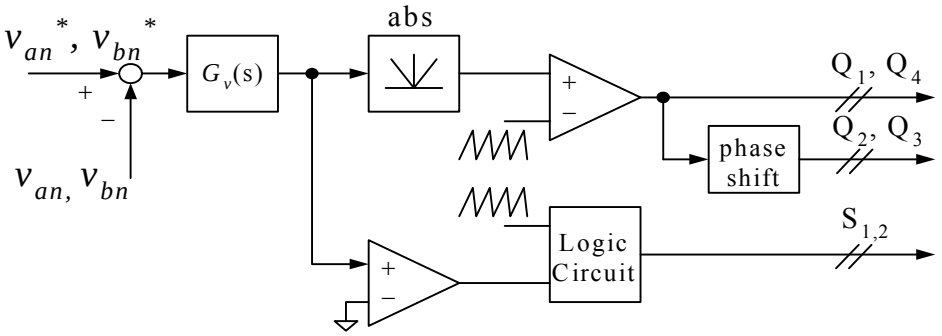

(a)

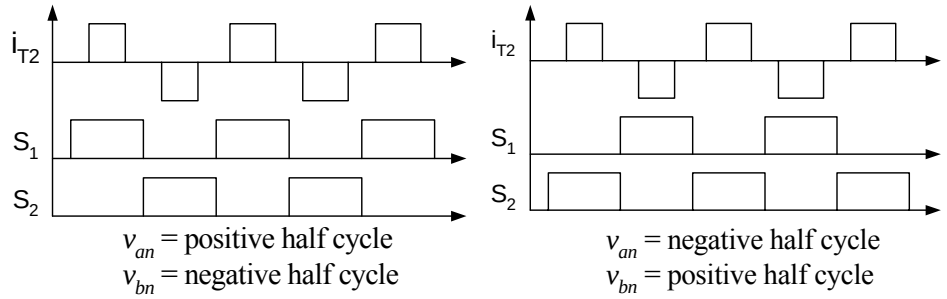

(b)

Fig. 4.5 Voltage control for current-fed high frequency link dc-ac converter. (a) Voltage control scheme. (b) Switching method of bi-directional switches.

The bi-directional switches S_1, S_2 in the secondary side are turned on with fixed duty ratio according to the polarities of the control input and link current, and switched to each other with a commutation for the leakage current of transformer as shown in Fig. 4.5 (b). Fig. 4.6 shows the current control scheme for the primary inductor. The inductor current is controlled by choosing the reset or restoring mode. The current reference can be calculated from the average output power. An integrator with a reset is used as a controller. The reset mode is selected $x_k > 0$ and the restoring mode is selected when $x_k<0$, where $x_k = \int_{(k-1)T}^{kT} [i^*_{Ls}(t) - i_{Ls}(t)]dt$ and T is the switching period.

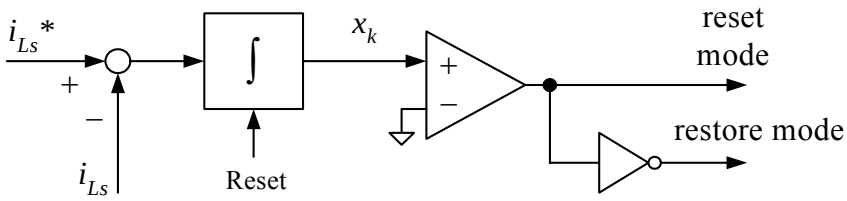

Fig. 4.6 Current control scheme for the primary inductor.

4.4.2 Control of active harmonic filter

Fig. 4.7 shows the control block diagram for the active harmonic filter. The current reference i_{Lf}^* can be calculated from the average output power P_{av} as shown in this figure.

The proportional-integral (PI) control is used for the block G_f(s). The control input is applied to the switches by using the PWM. As mentioned, there are two operating modes in the active filter. The buck mode is selected for the positive control

input while the boost mode for the negative control input. The switch Q_5 is controlled in the buck mode and Q_6 is controlled in the boost mode.

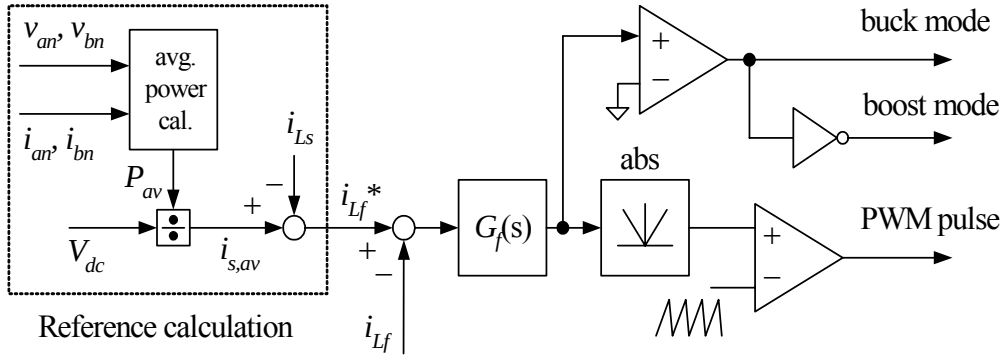

Fig. 4.7 Control block diagram of active harmonic filter.

4.5 Analysis of simulation results

To verify the usefulness of the proposed converter, the computer simulation is carried out for the actual parameters as follows: V_{dc} = 48V, f_s = 20kHz, L_s = 500uH, L_f = 500uH, C_{an} = C_{bn}= 50uF, C_f = 5600uF, n = 4, where f_s and n denote the switching frequency and transformer turn ratio, respectively. Fig. 4.8 shows the simulation results of the proposed high frequency link direct dc-ac converter for the balanced resistive load. It is shown in this figure that the proposed current-fed high frequency link direct converter produces the desired output voltages with high quality. Fig. 4.8 (b), (c), (d), and (e) represent the operation of the active harmonic filter, and shows the primary inductor current (i_{Ls}), filter inductor current (i_{Lf}), input current (i_s), and filter capacitor voltage (V_{cf}), respectively. It is noted in these figures that the harmonic current of 120Hz is effectively eliminated by employing the proposed active harmonic filter.

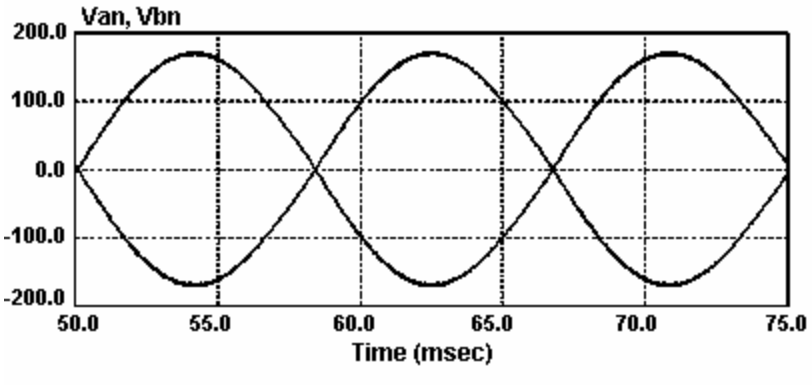

(a)

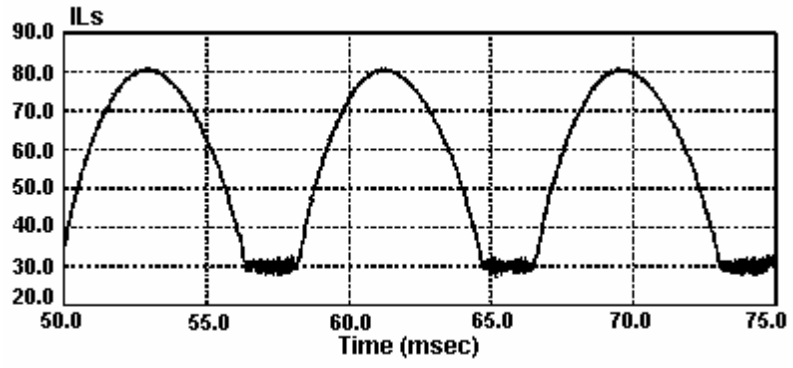

(b)

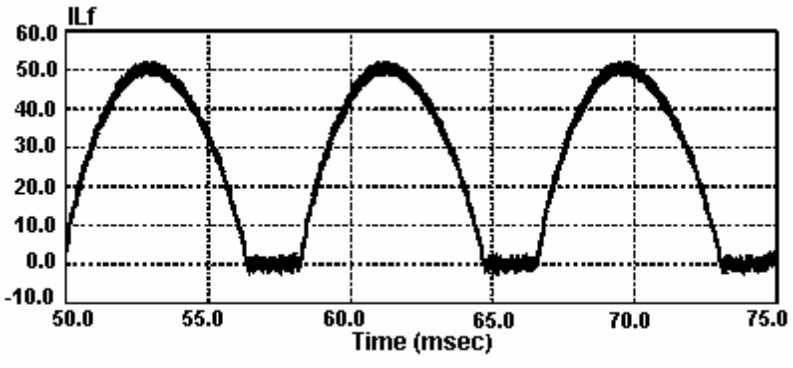

(c)

Fig. 4.8 Simulation results of proposed dc-ac converter for resistive load ($R_{an} = R_{bn} =$ 20Ω). (a) v_{an}, v_{bn}. (b) i_{Ls}. (c) i_{Lf}. (d) i_s. (e) v_{cf}.

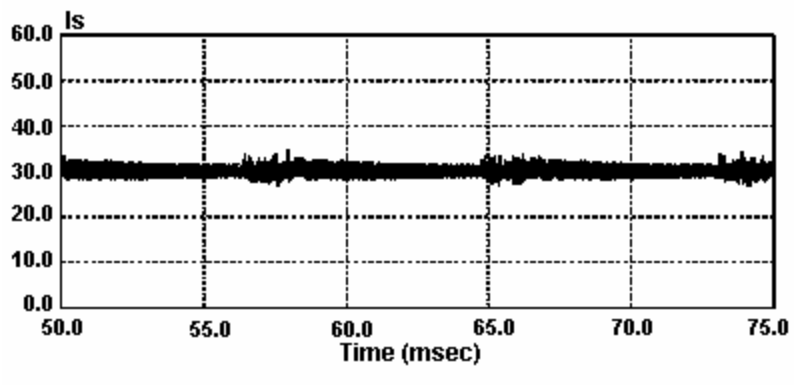

(d)

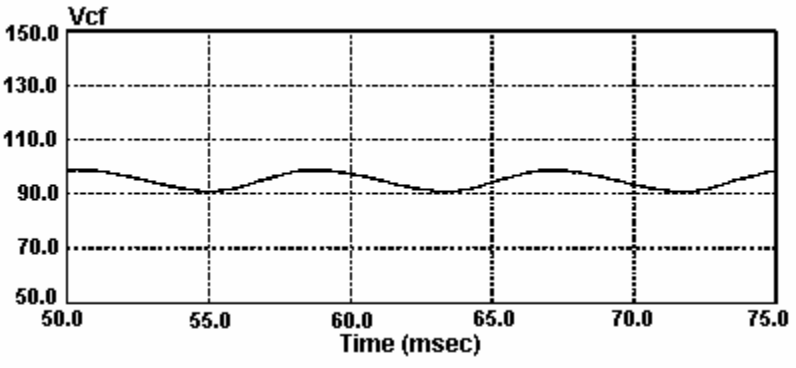

(e)

Fig. 4.8 Continued.

The simulation results for the unbalanced load are presented in Fig. 4.9, which shows that the proposed scheme operates properly in case of the unbalanced load. Fig. 4.10 shows the simulation results for the non-linear load. It is shown in the presented simulation results that the proposed high frequency link dc-ac converter provides the output voltage waveforms with high quality and eliminates the 120Hz input harmonic current drawn from the fuel cell effectively.

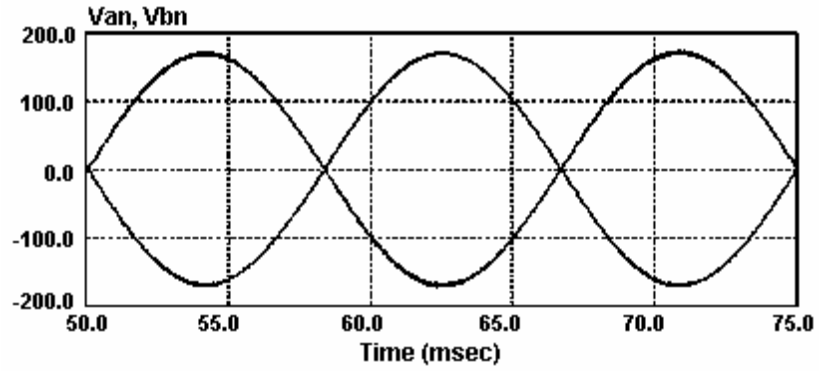

(a)

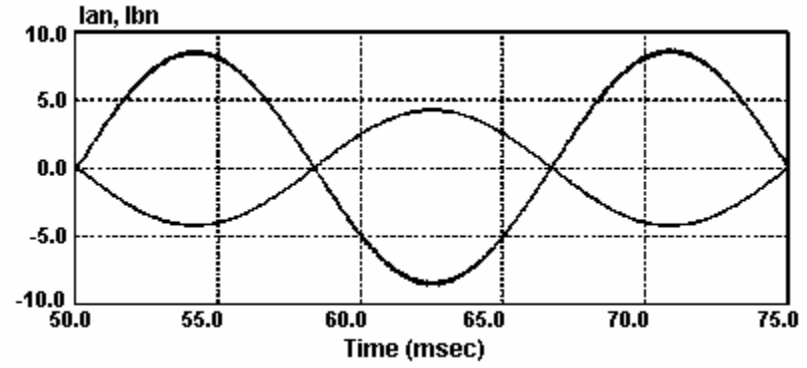

(b)

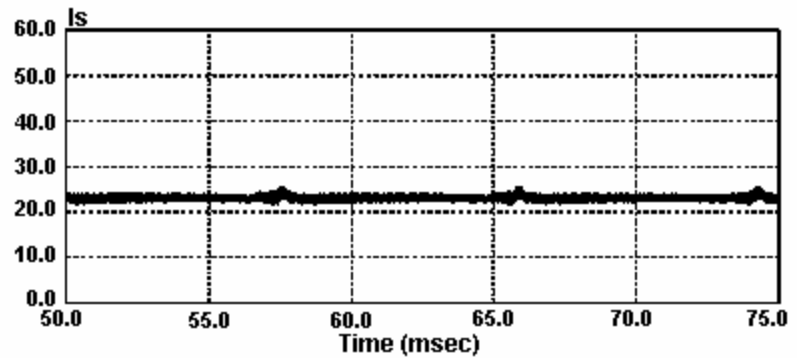

(c)

Fig. 4.9 Simulation results of proposed dc-ac converter for unbalanced load (R_{an} = 20Ω, R_{bn} = 40Ω). (a) v_{an}, v_{bn}. (b) i_{an}, i_{bn}. (c) i_s.

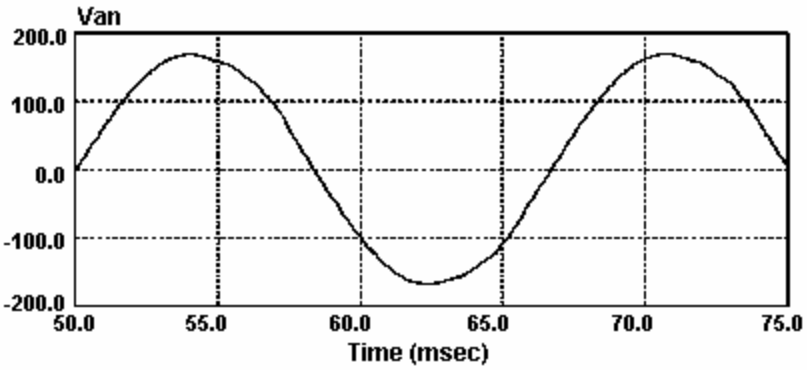

(a)

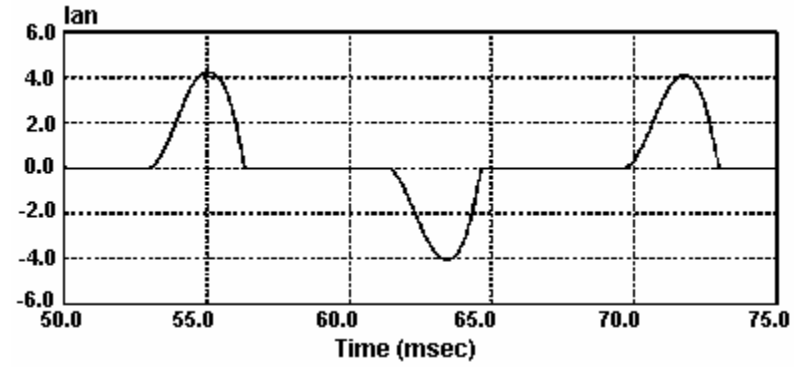

(b)

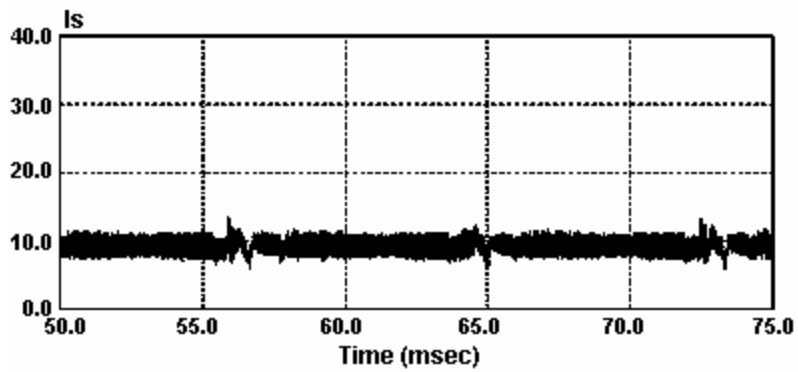

(c)

Fig. 4.10 Simulation results of proposed dc-ac converter for non-linear load. (a) v_{an}. (b) i_{an}. (c) i_s.

4.6 Conclusion

This chapter has presented a new current-fed high frequency link direct dc-ac converter with the capability of the 120Hz harmonic rejection for fuel cell applications. The current-fed high link direct dc-ac converter generates the split single phase ac outputs with high quality, and the active harmonic filter with an electrolytic capacitor effectively eliminates the input current ripple of 120Hz drawn from the fuel cell. The operation of the high frequency link dc-ac converter and harmonic filter has been investigated in detail. The simulation results well verify the validity of the proposed converter with the active filter, and show that the proposed scheme can be a good solution for the residential fuel cell power generation systems.

CHAPTER V

CONCLUSIONS

5.1 Conclusions

In this dissertation, new high frequency link power conversion systems for the fuel cell power conditioning have been proposed in order to improve performance and optimize the cost, size and weight of the power conversion systems, and their performance of the proposed schemes was verified by the various simulation and experiment results.

The bidirectional power flow, full-bridge dc-dc converter is applicable to the buck/boost converter to charge a battery or a supercapacitor during reverse power flow, which has attractive features in terms of low device stress, small filter components, low switching losses and simple first order dynamics. In the second chapter, a new soft switching technique using variable switching duty ratio for the bi-directional power flow full-bridge dc-dc converter was proposed. The proposed technique has been shown to achieve soft switching operation over wide load range. The proposed soft switching technique is also applicable to unidirectional dc-dc converter consisting of a full-bridge converter on the primary side and a diode rectifier and output filter on the secondary side.

A boost converter cascaded high frequency link direct dc-ac converter for fuel cell power sources has been proposed to provide a solution to build a compact power conversion system with high efficiency for distributed power system with fuel cell. The

boost converter has been shown to regulate the dc bus voltage effectively when the fuel cell voltage varies widely depending on the load condition. Further, the proposed multi-loop control of the boost converter has been shown to reduce the 120Hz input current harmonic drawn from the fuel cell to less than 10% without additional filter requirements. The evaluation of proposed PWM technique illustrates that immunity to voltage ripple at the dc bus can be achieved only at the expense of loss of voltage gain in the dc-ac converter and marginal dc current distortion. Experimental results have been shown to validate the feasibility of the proposed approach.

The fourth chapter has presented a new current-fed high frequency link direct dc-ac converter with the capability of the 120Hz harmonic rejection for fuel cell applications. The current-fed high link direct dc-ac converter generates the split single phase ac outputs with zero current switching, and the active harmonic filter with an electrolytic capacitor effectively eliminates the input current ripple of 120Hz drawn from the fuel cell to improve the performance of fuel cell system. The operation of the high frequency link dc-ac converter and harmonic filter has been investigated in detail. The simulation results well verify the validity of the proposed converter with the active filter, and show that the proposed scheme can be a good solution for low power fuel cell power generation systems.

5.2 Suggestions for further work

A bidirectional power flow, full-bridge dc-dc converter: a new soft switching technique was proposed. Further work is needed to control power flow in forward or in

reverse by proper switching of two active full-bridge converters and using the leakage inductance of transformer as an energy storage element.

High frequency link direct dc-ac converter: Further work is needed to design new soft switching scheme for the front-end boost converter and high frequency link dc-ac converter to reduce switching losses, and to investigate new approach to compensate the slow dynamics of fuel cell and the feasibility to extend the topologies to three-phase system.

REFERENCES

[1] H. Yonemori, T. Kominami, M. Nakaoka and M. Nishimura, “A new bidirectional series-resonant high-frequency linked power conversion system incorporating instantaneous sinewave-modulated regulation scheme,” in *Proc. Rec. IEEE IAS*, vol. 1, 1989, pp. 1015 – 1022.

[2] P. Sood, “High-frequency link power conversion system,” Ph.D dissertation, University of Wisconsin-Madison, Madison, Wisconsin, 1987.

[3] E. Santi, D. Franzoni, A. Monti, D. Patterson, F. Ponci and N.A. Barry, “Fuel cell based domestic uninterruptible power supply,**”** in *Proc. IEEE APEC*, vol. 1, 2002, pp. 605 – 613.

[4] Online fuel cell resources website, http://www.fuelcells.org/basics/how.html: accessed on May 11, 2004.

[5] K. Rajashekara, “Propulsion system strategies for fuel cell vehicle,” paper presented at SAE 2000 World Congress, Detroit, Michigan, March, 2000.

[6] T. Kawabata, “High frequency link DC/AC converter with PWM cycloconverter,” in *Proc. Rec. IEEE IAS*, vol. 2, 1990, pp. 1119 – 1124.

[7] G. K. Andersen, C. Klumpner, S. B. Kjaer and F. Blaabjerg, “A new green power inverter for fuel cells,” in *Proc. IEEE PESC’02*, vol. 2, 2002, pp. 727 – 733.

[8] P. Enjeti, “Development of a low cost fuel cell inverter system with DSP control,” in *Proc. IEEE PESC’02*, vol. 2, 2002, pp. 309 – 314.

[9] A. M. Tuckey and J. N. Krase, ”A low-cost inverter for domestic fuel cell applications,” in *Proc. IEEE PESC’02*, vol. 1, 2002, pp. 339 – 346.

[10] P. T. Krein and R. Balog, “Low cost inverter suitable for medium-power fuel cell sources,” in *Proc. IEEE PESC’02*, vol. 1, 2002, pp. 321 – 326.

[11] V. T. Ranganathsn, P. D. Ziogas and V. R. Stefanovic, ”A DC-AC power conversion technique using twin resonant high-frequency links,” *IEEE Trans. Ind. Applicat*., vol. IA-19, May/June 1983, pp. 393-400.

[12] I. Yamato, N. Tokunaga, Y. Matsuda, H. Amano, and Y. Suzuki, “New conversion system for UPS using high frequency link,” in *Proc. Rec. IEEE PESC’88*, April, 1988, pp. 658-663.

[13] M. Matsui, M. Nagai, M. Mochizuki and A. Nabae, ”High-frequency link DC/AC converter with suppressed voltage clamp circuits-naturally commutated phase angle control with self turn-off devices,” *IEEE Trans. Ind. Applicat*., vol. 32, no. 2, March/April 1996, pp. 293-300.

[14] M. H. Kheraluwala, R. W. Gascoigne and D. M. Divan, ”Performance characterization of a high-power dual active bridge,” *IEEE Trans. Ind. Applicat.*, vol. 28, no. 6,1992, pp. 1294-1301.

[15] H. L. Chan, K. W. E. Cheng, and D.Sutanto, ”A novel square-wave converter with bi-directional power flow,” in *Proc. Rec. IEEE PEDS’99*., 1999, vol. 2, pp. 966-971.

[16] G. Hua, F. C. Lee and M. M. Jovanovic, ”An improved full-bridge zero-voltage-switched PWM converter using a saturable inductor,” *IEEE Trans. Power Electronics*, vol. 8, Oct. 1993, pp. 530-534.

[17] E. S. Kim, K. Y. Joe, M. H. Kye and B. D. Yoon, ”An improved soft-switching PWM FB DC/DC converter for reducing conduction losses,” *IEEE Trans. Power*

Electronics, vol. 14, no. 2, March 1999, pp. 258-264.

[18] R. Ayyanar and N. Mohan, ”Novel soft switching DC-DC converter with full ZVS-range and reduced filter requirement. I. Regulated –output applications,” *IEEE Trans. Power Electronics*, vol. 16, March 2001, pp. 184-192.

[19] H. L. Chan, K.W.E. Cheng, and D. Sutanto, ”An extended load range ZCS-ZVS bi-directional phase-shifted DC-DC converter,” in *Proc. Rec. IEEE PEVSD*, 2000, vol. 2, pp. 74-79.

[20] Dept of Energy, *2001 Future Energy Challenge Final Report*, http://www.energychallenge.org.

[21] T. A. Nergaard, J. F. Ferrell, L. G. Leslie, and J.S. Lai, “Design considerations for a 48V fuel cell to split single phase inverter system with ultracapacitor energy storage,” in *Proc. Rec. IEEE PESC’02*, pp. 2007-2012.

[22] G. K. Andersen, C. Klumpner, S. B. Kjar and F. Blaabjerg, “A new green power inverter for fuel cells,” in *Proc. Rec. IEEE PESC’02*, pp. 727-733.

[23] P. T. Krein and R. Balog, “Low cost inverter suitable for medium-power fuel cell sources,” in *Proc. Rec. IEEE PESC’02*, pp. 321-326.

[24] D. M. Divan, “The resonant DC link converter- a new concept in static power conversion,” *IEEE Trans. Ind. Applicat*., vol. 25, March-April 1989, pp. 317-325.

[25] M. H. Todorovic, L. Palma and P. Enjeti, “Design of a wide input range DC-DC converter with a robust power control scheme suitable for fuel cell power conversion,” in *Proc. IEEE APEC*, 2004, pp. 374-379.

[26] R. S. Gemmen, “Analysis for the effect of inverter ripple current on fuel cell operation condition,” in *ASME’01 International Mechanical Engineering*

Congress and Exposition, Pittsburgh, PA, Nov.11-16 2001.

[27] Dept of Energy, *Future Energy Challenge, 2001 and 2003*, http://www.energychallenge.org: accessed on May 11, 2004.

[28] P. Enjeti and W. Shireen, "A new technique to reject DC-link voltage ripple for inverters operating on programmed PWM waveforms," *IEEE Trans. Power Electronics*, vol. 7, no.1,1992, pp.171-180.

[29] P. N. Enjeti and S. Choi, "An approach to realize higher power ac controller," in *Proc. IEEE APEC*, 1993, pp. 323-327.

[30] M. Kang, P. N. Enjeti, and I. J. Pitel, "Analysis and design of electronic transformers for electric power distribution system," in *IEEE Trans. Power Electronics*, vol. 14, no. 6, Nov. 1999, pp. 1133-1141.

[31] P. Tenti, L. Rossetto, L. Malesani, R. Borgatti, and R. Stefani, "Single-stage current-fed DC/DC converter with time-sharing control of output voltage and input current," *IEEE Trans. Power Electronics*, vol. 5, no. 4, 1990, pp.389-397.

[32] P. J. Wolf, K. C. Kwong, and G. F. Ledwich, "A single-phase converter with a high-frequency current-sourced link," *IEEE Trans. Power Electronics*, vol. 7, no. 4, 1992, pp. 683-692.

[33] K. Tazume, T. Aoki, and T. Yamashita, "Novel method for controlling a high-frequency link inverter," in *Proc. Rec. IEEE PESC'98*, pp. 497-502.

[34] T. Larsson, S. Ostlund, and F. Gustavson, "An active DC link filter for AC-AC converters," in *Proc. Rec. IEEE PEVSD*, 1994, pp.331-335.

[35] O. H. Stielau, J. D. van Wyk and J. J. Schoeman, "A high density three-phase high frequency link system for variable frequency," in *Proc. Rec. IEEE IAS*, Oct.

1989, pp. 1031-1036.

[36] C. Liu, T. Nergaard, L. Leslie, J. Ferrell, X. Huang, T. Shearer, J. Reichl, J. Lai and J. Bates, “Power balance control and voltage conditioning for fuel cell converter with multiple sources,” in *Proc. Rec. PESC’02*, vol. 4, pp. 2001-2006.

[37] M. J. Gorman and M.E. Elbuluk, “A simple two-switch cycloconverter for variable-frequency low speed application,” *IEEE Trans. Ind. Applicat.*, vol. 6, no. 4, Oct. 1991, pp. 759-764.

[38] P. J. Wolfs. G. F. Ledwich and K. C. Kwong, “The application of the duality principle to nonplanar circuits,” *IEEE Trans. Power Electronics*, vol. 8, Apr. 1993, pp. 104-111.

VITA

Yu Jin Song received his B.S. and M.S. degree in electrical engineering from Yonsei University, Seoul, Korea in 1988 and 1991. He worked on the development of the digital control system in Daewoo Heavy Industry from 1991 to 1997. He started the Ph.D. program in electrical engineering at Texas A&M University in the Fall of 1999 and received his Ph.D. in August 2004. He worked as a Research Assistant in the Power Electronics and Power Quality Laboratory of the Electrical Engineering Department, conducting research on design of high frequency link power conversion system for distributed power system and power quality issues. His research interests are primarily in advanced power electronics converters applied to distributed power system with renewable energy sources, power quality issues and soft switching technique.

He can be reached via Dr. Prasad Enjeti [enjeti@tamu.edu (979-845-7466)] or via eugenesong2000@yahoo.com. His permanent address in his hometown is: 59 Songhyun, Jinlae-myun, Kimhae-shi, Gyoungnam 600-88, Korea.